also ill-shaped. The left posterior inferior temporal gyrus is known to be associated with Japanese pure agraphia, limited to kanji recall [19, 31]. In our study, performance in kanji dictation was significantly impaired in the patients compared to the controls. However, we think the lesion was not responsible because errors in kana were more frequently noted in the composition. The patients showed equal impairment in both kana and kanji recall.

Satoh [28] reported that 3 of 16 ALS patients without dementia had a tendency to omit kana in dictation. The subjective dictation words consisted of 2–5 kana letters each, and if a word contained three or more kana letters, the likelihood of the patient omitting letters was greater. They also described some patients who showed kanji agraphia. Ichikawa et al. [15] recently reported that bulbar-onset ALS patients showed high prevalence of agraphia characterized by omission, substitution of kana, and misuse of postposition. They reported the details of patients in a series of two Japanese reports. While they emphasized kana-error represented by omission, they also illustrated patients having kanji-dominant writing error [12, 14]. Errors of kana and kanji were independent of each other in many patients and they speculated that writing errors of ALS patients might be classified into two types arising from different lesions, as FTLD has two types of aphasia, progressive aphasia and semantic dementia.

Agraphia was also reported in many cases of primary lateral sclerosis (PLS) [25, 34]. Similar to our study, the pattern of errors varied from agrammatism to misspelling. In a study on PLS, it was found that words containing less than five letters were spelt correctly; thus, the length of a word affects misspelling. On the basis of the strong association between misspelling and severity of dysarthria (bulbar part of ALSFRS-R), the researchers proposed that it was because of a deficit in rehearsal for spelling when subjects could not speak. Ichikawa, et al. [15] pointed out that agraphia was frequently noted in patients with bulbar-onset ALS. They did not mention limb-onset ALS. In our study, however, WEI and the bulbar part of the ALSFRS-R were not correlated; thus, the results did not support the rehearsal theory. Because only a few patients of the limb-onset group could perform writing tests in this study, it is unclear whether agraphia is specific to bulbar-onset patients. We think that agraphia was independent of motor disability.

Difficulty in PA was another characteristic of ALS. PA in WAIS-III reflected performance IQ, but because it is a complex task, PA was not classified into specific secondary indices. Further, PA was excluded from WAIS-IV. Only a few reports have described what poor performance in PA implies. In psychiatric disorders, PA and explanation of the story have been considered to be associated with social cognition [2, 30]. However, PA requires more complex factors than social cognition. To understand each picture, social cognition represented by speculation of relationships, social experiences, knowledge of behavior, and insight into others' emotions is required. Moreover, for PA, speculation of time sequence and working memory is necessary. Both defects in social cognition and working memory are critical features of frontotemporal dementia. In the present study, PA was scored from 0 to 3 points, and the patients were clearly divided into two groups: those who could perform the task easily (3 or 2 points) and those who could not (0 or 1 points, sometimes 2 points but with long consideration). PA might be useful for screening of mild cognitive disturbance associated with ALS. Moreover, PA and WEI were highly correlated. Confusion of a story line as determined from the uncorrected picture sequence could affect the WEI, but the result that the subject of the picnic picture (WAB IV; composition) had the same tendency of error showed that the mistakes were not because of the uncorrected sequences.

Impairment in PA and agraphia might be the most sensitive symptoms of mild cognitive impairment. According to the consensus criteria for cognition in ALS patients, tests should be completed within 20 min [32]. PA involving the arrangement of one set of pictures is easy to perform within 3 min.

Recent findings on the accumulation of TAR-DNA binding protein 43 kDa (TDP-43) both in ALS and FTD patients further support the notion of a common pathway for both these diseases [4, 18, 22]. On the other hand, in the case of patients who undergo long-term mechanical ventilation and show a modest extra-motor lesion, extension of the extra-motor pathology is not affected by either severity of the motor symptom or disease duration [23]. In the present study, some patients were cognitively intact, and the patient with the best WEI had the worst ALSFRS-R. The disagreement between motor function and agraphia also supports this view, and the writing examination might be a sensitive indicator of the future possibility of cognitive involvement. Therefore, patients with agraphia need to be carefully observed with regard to progression of their condition to dementia.

Acknowledgments We thank all the patients and control subjects for their active cooperation. This work was supported by Grants-in-Aid from the Research Committee of CNS Degenerative Diseases, the Ministry of Health, Labour and Welfare of Japan.

Conflict of interest The authors report no conflicts of interest.

References

1. Abrahams S, Goldstein LH, Simmons A, Brammer M, Williams SC, Giampietro V, Leigh PN (2004) Word retrieval in amyotrophic lateral sclerosis: a functional magnetic resonance imaging study. Brain 127:1507–1517

2. Allen DN, Strauss GP, Donohue B, van Kammen DP (2007) Factor analytic support for social cognition as a separable cognitive domain in schizophrenia. Schizophr Res 93:325–333
3. Anderson SW, Damasio AR, Damasio H (1990) Troubled letters but not numbers. Domain specific cognitive impairments following focal damage in frontal cortex. Brain 113(Pt 3):749–766
4. Arai T, Hasegawa M, Akiyama H, Ikeda K, Nonaka T, Mori H, Mann D, Tsuchiya K, Yoshida M, Hashizume Y, Oda T (2006) TDP-43 is a component of ubiquitin-positive tau-negative inclusions in frontotemporal lobar degeneration and amyotrophic lateral sclerosis. Biochem Biophys Res Commun 351:602–611
5. Basso A, Taborelli A, Vignolo LA (1978) Dissociated disorders of speaking and writing in aphasia. J Neurol Neurosurg Psychiatry 41:556–563
6. Baxter DM, Warrington EK (1986) Ideational agraphia: a single case study. J Neurol Neurosurg Psychiatry 49:369–374
7. Brooks BR, Miller RG, Swash M, Munsat TL (2000) El Escorial revisited: revised criteria for the diagnosis of amyotrophic lateral sclerosis. Amyotroph Lateral Scler Other Motor Neuron Disord 1:293–299
8. Caselli RJ, Windebank AJ, Petersen RC, Komori T, Parisi JE, Okazaki H, Kokmen E, Iverson R, Dinapoli RP, Graff-Radford NR et al (1993) Rapidly progressive aphasic dementia and motor neuron disease. Ann Neurol 33:200–207
9. Cedarbaum JM, Stambler N, Malta E, Fuller C, Hilt D, Thurmond B, Nakanishi A (1999) The ALSFRS-R: a revised ALS functional rating scale that incorporates assessments of respiratory function. BDNF ALS Study Group (Phase III). J Neurol Sci 169:13–21
10. Ferrer I, Roig C, Espino A, Peiro G, Matias Guiu X (1991) Dementia of frontal lobe type and motor neuron disease. A Golgi study of the frontal cortex. J Neurol Neurosurg Psychiatry 54:932–934
11. Heilman K (2003) clinical neuropsychology. Oxford university press, Oxford
12. Ichikawa H, Kawamura M (2010) Language impairment in amyotrophic lateral sclerosis. Brain Nerve 62:435–440
13. Ichikawa H, Koyama S, Ohno H, Ishihara K, Nagumo K, Kawamura M (2008) Writing errors and anosognosia in amyotrophic lateral sclerosis with dementia. Behav Neurol 19:107–116
14. Ichikawa H, Takahashi N, Hieda S, Kawamura M (2010) Bulbar-onset amyotrophic lateral sclerosis (ALS) with isolated agraphia. Rinsho Shinkeigaku 50:81–86
15. Ichikawa H, Takahashi N, Hieda S, Ohno H, Kawamura M (2008) Agraphia in bulbar-onset amyotrophic lateral sclerosis: not merely a consequence of dementia or aphasia. Behav Neurol 20:91–99
16. Kanzaki M, Sato M, Ogawa G, Miyamoto N, Motoyoshi K, Kamakura K, Takeda K (2004) A case of dementia with motor neuron disease associated with agraphia—the omission of kana letters. Rinsho Shinkeigaku 44:673–676
17. Lomen-Hoerth C, Murphy J, Langmore S, Kramer JH, Olney RK, Miller B (2003) Are amyotrophic lateral sclerosis patients cognitively normal? Neurology 60:1094–1097
18. Mackenzie IR, Bigio EH, Ince PG, Geser F, Neumann M, Cairns NJ, Kwong LK, Forman MS, Ravits J, Stewart H, Eisen A, McClusky L, Kretzschmar HA, Monoranu CM, Highley JR, Kirby J, Siddique T, Shaw PJ, Lee VM, Trojanowski JQ (2007) Pathological TDP-43 distinguishes sporadic amyotrophic lateral sclerosis from amyotrophic lateral sclerosis with SOD1 mutations. Ann Neurol 61:427–434
19. Mochizuki H, Ohtomo R (1988) Pure alexia in Japanese and agraphia without alexia in kanji. The ability dissociation between reading and writing in kanji vs. kana. Arch Neurol 45:1157–1159
20. Murphy JM, Henry RG, Langmore S, Kramer JH, Miller BL, Lomen-Hoerth C (2007) Continuum of frontal lobe impairment in amyotrophic lateral sclerosis. Arch Neurol 64:530–534
21. Neary D, Snowden JS, Gustafson L, Passant U, Stuss D, Black S, Freedman M, Kertesz A, Robert PH, Albert M, Boone K, Miller BL, Cummings J, Benson DF (1998) Frontotemporal lobar degeneration: a consensus on clinical diagnostic criteria. Neurology 51:1546–1554
22. Neumann M, Mackenzie IR, Cairns NJ, Boyer PJ, Markesbery WR, Smith CD, Taylor JP, Kretzschmar HA, Kimonis VE, Forman MS (2007) TDP-43 in the ubiquitin pathology of frontotemporal dementia with VCP gene mutations. J Neuropathol Exp Neurol 66:152–157
23. Nishihira Y, Tan CF, Onodera O, Toyoshima Y, Yamada M, Morita T, Nishizawa M, Kakita A, Takahashi H (2008) Sporadic amyotrophic lateral sclerosis: two pathological patterns shown by analysis of distribution of TDP-43-immunoreactive neuronal and glial cytoplasmic inclusions. Acta Neuropathol 116:169–182
24. Otsuki M, Soma Y, Arai T, Otsuka A, Tsuji S (1999) Pure apraxic agraphia with abnormal writing stroke sequences: report of a Japanese patient with a left superior parietal haemorrhage. J Neurol Neurosurg Psychiatry 66:233–237
25. Piquard A, Le Forestier N, Baudoin-Madec V, Delgadillo D, Salachas F, Pradat PF, Derouesne C, Meininger V, Lacomblez L (2006) Neuropsychological changes in patients with primary lateral sclerosis. Amyotroph Lateral Scler 7:150–160
26. Ringholz GM, Appel SH, Bradshaw M, Cooke NA, Mosnik DM, Schulz PE (2005) Prevalence and patterns of cognitive impairment in sporadic ALS. Neurology 65:586–590
27. Sakurai Y, Matsumura K, Iwatsubo T, Momose T (1997) Frontal pure agraphia for kanji or kana: dissociation between morphology and phonology. Neurology 49:946–952
28. Satoh M, Takeda K, Kuzuhara S (2009) Agraphia in intellectually normal Japanese patients with ALS: omission of kana letters. J Neurol 256:1455–1460
29. Seki R, Ishiai S, Koyama Y, Sato S, Seki K (2000) Aphasia and paragraphia of kana letters following infarction in the posterior middle and inferior frontal gyri. Japanese J Neuropsychol 16:127–134
30. Shean G, Meyer J (2009) Symptoms of schizophrenia and social cognition. Psychiatry Res 170:157–160
31. Soma Y, Sugishita M, Kitamura K, Maruyama S, Imanaga H (1989) Lexical agraphia in the Japanese language. Pure agraphia for Kanji due to left poster inferior temporal lesions. Brain 112 ((Pt 6)):1549–1561
32. Strong MJ, Grace GM, Freedman M, Lomen-Hoerth C, Woolley S, Goldstein LH, Murphy J, Shoesmith C, Rosenfeld S, Leigh PN, Bruijn L, Ince PG, Figlewicz D (2009) Consensus criteria for the diagnosis of frontotemporal cognitive and behavioural syndrome in amyotrophic lateral sclerosis. Amyotroph Lateral Scler 10:131–146
33. Tohgi H, Saitoh K, Takahashi S, Takahashi H, Utsugisawa K, Yonezawa H, Hatano K, Sasaki T (1995) Agraphia and acalculia after a left prefrontal (F1, F2) infarction. J Neurol Neurosurg Psychiatry 58:629–632
34. Zago S, Poletti B, Corbo M, Adobbati L, Silani V (2008) Dysgraphia in patients with primary lateral sclerosis: a speech-based rehearsal deficit? Behav Neurol 19:169–175

Neuroscience Letters 452 (2009) 52–55

Contents lists available at ScienceDirect

Neuroscience Letters

journal homepage: www.elsevier.com/locate/neulet

Cystatin C in cerebrospinal fluid as a biomarker of ALS

Sachiko Tsuji-Akimoto[a,*], Ichiro Yabe[a,1], Masaaki Niino[a,1], Seiji Kikuchi[b,2], Hidenao Sasaki[a,1]

[a] Department of Neurology, Graduate School of Medicine, Hokkaido University, Kita 15 Nishi 7, Kita-ku, Sapporo City, Hokkaido, Japan
[b] Department of Neurology, Sapporo Minami Hospital, National Hospital Organization, Shirakawa 1814, Minami-ku, Sapporo City, Hokkaido, Japan

ARTICLE INFO

Article history:
Received 15 August 2008
Received in revised form 9 January 2009
Accepted 9 January 2009

Keywords:
Amyotrophic lateral sclerosis
Cystatin C
Diagnosis
Biomarker

ABSTRACT

Amyotrophic lateral sclerosis (ALS) is diagnosed on the basis of progressive symptoms in both the upper and lower motor neurons. Because there are no specific biomarkers for ALS, it is difficult to diagnose this disease in its early stages. Cerebrospinal fluid (CSF) samples were obtained from 14 patients in the early stages of ALS, from 13 with polyneuropathy, and from 16 with other neurological disorders. The concentration of cystatin C in the CSF was measured using a sandwich enzyme-linked immunosorbent assay (ELISA) kit. The concentration of cystatin C in the CSF was significantly lower in ALS patients than in the control subjects who were patients with polyneuropathy or other neurological diseases (patients with ALS, polyneuropathy, and other diseases exhibited 5.5 ± 0.3, 6.7 ± 0.4, and 6.9 ± 0.3 mg/L cystatin C, respectively; ALS patients vs. control subjects: $p = 0.014$ and ALS patients vs. polyneuropathy patients: $p = 0.024$). Cystatin C may be a useful biomarker of ALS and can be used to distinguish between ALS and polyneuropathy.

Amyotrophic lateral sclerosis (ALS) is a neurodegenerative disorder characterized by the specific degeneration of motor neurons. The following are critical points that are considered for the clinical diagnosis of ALS: (1) progressive course, (2) enlarging lesions (3) involvement of both the upper and lower motor neurons, and (4) exclusion of other diseases. According to the revised El Escorial Criteria (rEEC), which are the international criteria for the diagnosis of ALS, diagnostic accuracy is determined on the basis of the distribution and combination of symptoms of the disease in the upper and lower motor neurons [7]. According to rEEC, ALS is divided into five categories: definite, probable, clinically probable or laboratory supported, possible, and suspected. Currently, these are the most reliable criteria for diagnosis when specific biomarkers are not frequently detected, and as recommended by the World Federation of Neurology, many clinical trials are performed on individuals diagnosed with definite, probable, and clinically probable cases of ALS.

However, it is often difficult to diagnose ALS. In many patients, the first symptoms occur in a single area and remain restricted there for months. Such patients are diagnosed with possible ALS, and they do not participate in clinical trials unless their condition deteriorates. Indeed, the mean intervals from the time of the first symptom to the time of diagnosis in three population-based studies were 8 [34], 10.6 [3] and 14.4 months [36]. Among the 34 cases of ALS that were diagnosed on the basis of the autopsy findings, the average duration between the onset of ALS symptoms and the diagnosis of definite ALS was 21 months [6]. Thus, it is important to determine the correct stage at which ALS should be diagnosed. Furthermore, when symptoms are widely distributed, 16% of ALS patients diagnosed by clinical physicians exhibited only lower motor neuron symptoms throughout their life, which satisfies the definition of clinically suspected ALS alone [34]. It is often difficult to differentiate ALS from other diseases. Two clinically instructive cohort studies demonstrated that 7–8% of patients diagnosed with ALS could be re-diagnosed with other diseases such as cervical spondylotic myeloradiculopathy, multifocal motor neuropathy (MMN), and spinobulbar muscular atrophy [9,33]. The rEEC permitted electromyography and gene analysis in addition to routine laboratory data and neuroradiological examinations. However, cases with poor electromyographic findings in nonsymptomatic muscles are frequently observed. In a retrospective electromyographic study in 82 patients suspected with ALS, the specificity was 0.97 and the sensitivity was 0.57 [18]. Gene analysis also has a low sensitivity, and it can be applied only to approximately 2% of all ALS patients, who have a mutation in the Cu^{2+}, Zn^{2+}-superoxide dismutases, which is the most frequent familial ALS [28]. Powerful diagnostic tools are required for the accurate diagnosis of possible or suspected ALS with a high sensitivity.

No specific biomarkers have yet been universally confirmed for ALS. However, a recent proteomic analysis revealed that cystatin C, transthyretin, and other protein species (4.8 and 6.7 kDa) in the cerebrospinal fluid (CSF) were possible biomarkers of ALS [25,26].

* Corresponding author. Tel.: +81 11 706 6028; fax: +81 11 700 5356.
E-mail address: tujitti@jb3.so-net.ne.jp (S. Tsuji-Akimoto).
[1] Tel.: +81 11 706 6028; fax: +81 11 700 5356.
[2] Tel.: +81 11 596 2211; fax: +81 11 596 3122.

0304-3940/$ – see front matter © 2009 Elsevier Ireland Ltd. All rights reserved.
doi:10.1016/j.neulet.2009.01.026

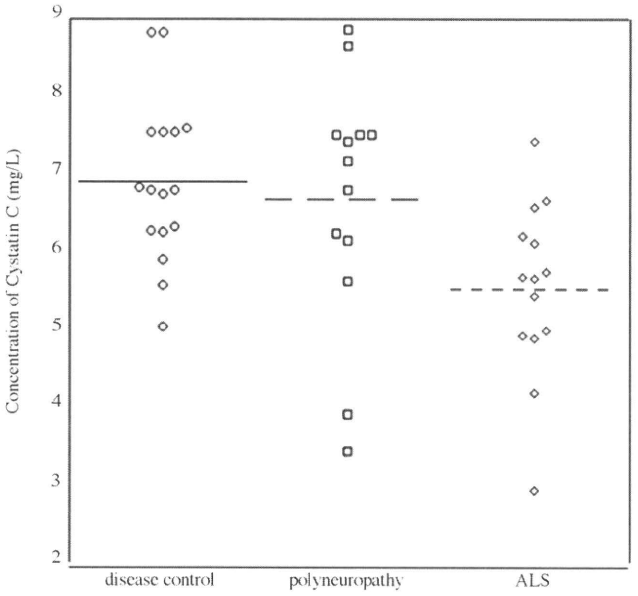

Fig. 1. Concentration of cystatin C in the CSF. The average concentration in the ALS group is significantly lower than that in the control groups (ALS patients vs. controls with other diseases: $p = 0.014$ and vs. controls with polyneuropathy: $p = 0.024$).

In particular, cystatin C may be a specific biomarker since it is specific for Bunina bodies, a characteristic feature of ALS [21]. Although ubiquitin-positive inclusions are a disease-specific pathology in various neurodegenerative disorders such as Parkinson's disease and multiple system atrophy [35], Bunina bodies are characteristic indicators of ubiquitin-negative protein accumulation. The process by which they are formed remains unknown; however, cystatin C and ferritin [19] have been recently identified using immunohistological methods.

In this study, we demonstrate that the presence of cystatin C in the CSF could be used as a clinical marker for the diagnosis of ALS in its early stages, especially to distinguish ALS from polyneuropathy.

CSF samples were obtained from 14 ALS patients who had undergone lumbar puncture at the Hokkaido University Hospital from April 2006 to March 2007. The controls were patients with polyneuropathy and other diseases and who were of the same sex and age as the ALS subjects. Meningitis and other acute inflammatory disorders that cause increases in the CSF cell count were excluded. Thirteen patients with polyneuropathy and 16 with other diseases were the control subjects; these patients were definitely diagnosed with polyneuropathy or other diseases. CSF samples from cases of neuropathy were obtained before medication. In the control group, the disease phase at the time of CSF collection varied. Patients who were categorized under the "suspect" group of ALS according to the rEEC were excluded from our study; however, patients from this group and those with possible ALS were included if the progressive course was confirmed after several months. Two patients with ALS symptoms only in the lower motor neurons underwent repetitive nerve conduction tests and intravenous immunoglobulin therapy (IVIg), but they did not show any improvement in the symptoms. Since the rEEC for the diagnosis of ALS is stringent, 16% of the patients were not diagnosed with ALS until the final stages of the disease. In Ireland, suspected and possible patients were included if the typical clinical course was confirmed prospectively, and other diseases were excluded [23]. International scales of the symptom, such as revised ALS functional rating scale (ALSFRS-R), were not available on all subjects at the lumber puncture; therefore correlation to clinical severity cannot be addressed. Informed consent was obtained from all the subjects for research purposes, and the study

Table 1
Profile of patients.

	Number of patients	Age (average ± S.D., years old)	Female/male
ALS	14	62 ± 10	2/12
Polyneuropathy	13	56 ± 18	2/11
Other disease control	16	64 ± 15	2/14

Sex- and age-matched patients were analyzed.

Table 2
Detail of each group.

Polyneuropathy	Number of patients
Chronic inflammatory demyelinating polyneuropathy	5
Multifocal motor neuropathy	3
Churg-Strauss syndrome	2
Charcot-Marrie-tooth disese	2
Cisplatin neuropathy	1
Other disease control	
Normal pressure hydrocephalus	7
Cervical spondylotic myelopathy	3
Post-cerebral infarction	2
Post-cerebral hemorrage	1
Ideopathic intracranial hypertension	1
Phenytoin toxication	1
Psychogenic reaction	1

Detailed diagnoses of control groups were shown.

was approved by the ethical committee of Hokkaido University.

The collected CSF samples were kept in 4 °C for several hours at longest, and after division into 1-mL of aliquots without centrifugation, they were preserved at −80 °C until they were used for analysis. The concentration of cystatin C was measured using sandwich enzyme-linked immunosorbent assay (ELISA) with a human cystatin C ELISA kit (Quantikine, R and D systems, Mckinley Place, NE, USA). A 40-fold dilution of the samples was prepared, and ELISA was performed according to the instructions provided in the kit. All samples were measured at single time. After colorization with tetramethylbenzidine, the absorbance was determined at 450 nm by using a microplate reader, and the wavelength used for correction was 570 nm. The results were analyzed using KaleidaGraph 4.0 software. Statistical analysis was performed using the Student–Newman–Keuls test when one-factorial analysis of variance (ANOVA) showed significance (Fig. 1).

Details of the patients are described in Tables 1–3. The mean age of ALS patients and the control subjects with polyneuropathy and other diseases were 62 ± 10, 56 ± 18, and 64 ± 15 years, respectively. The period between the onset of ALS and lumbar puncture was 9.9 months (range, 3–24 months). The female/male ratio of the 3 groups was 2/12, 2/11, and 2/14, respectively. After obtaining the CSF samples from the 8 patients who were diagnosed with possible and suspected ALS, 3 died from respiratory failure within 2 years after the lumbar puncture and 4 progressed to probable or definite ALS. The muscular atrophy and weakness of the remaining one patient who belonged to the "suspect" ALS category marked deteriorated though he was received repetitive IVIg therapies. The mean concentration of cystatin C was 5.5 ± 0.3 mg/L in the ALS group,

Table 3
Classification of rEEC on ALS.

Classification of rEEC on ALS	Number of patients
Definite	0
Probable	2
Clinically probable—laboratory-supported	4
Possible	5
Suspect	3

The classification of revised El Escorial Criteria (rEEC) when the CSF was obtained.

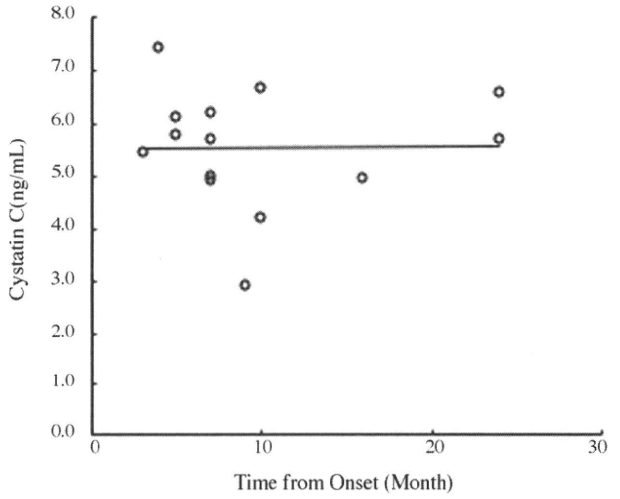

Fig. 2. The time from the onset of ALS was not related to the cystatin C concentration. Approximate line: $Y = 0.0028X + 5.55164$, Pearson's correlation coefficient: 0.017.

6.7 ± 0.4 mg/L in the polyneuropathy group, and 6.9 ± 0.3 mg/L in the other disease group. The concentration was found to be significantly lower in the ALS group than in the other two groups (ALS patients vs. other disease controls: $p = 0.014$ and ALS patients vs. polyneuropathy patients: $p = 0.024$).

Of the two control groups, no correlation was observed between the age and cystatin C concentration. In the ALS group, there was no correlation between the cystatin C concentration and the duration of the disease (Fig. 2). In the ALS group, 5 patients showed bulbar symptoms at the onset of ALS and 3 patients were classified as having progressive bulbar palsy. A slight reduction in the concentration of cystatin C was observed in these patients. Analysis of the CSF samples showed that the extent of the affected region, and the duration of the disease were not correlated with the concentration of cystatin C.

Three patients with cervical spondylotic myelopathy (CSM) and 3 with MMN were included in the control groups. These patients were frequently misdiagnosed with ALS. Although the sample size is small, their concentrations were not lower than the average concentration observed in ALS (individual concentrations of CSM: 8.8, 7.6, and 8.8 mg/L and individual concentrations of MMN: 6.8, 8.9, and 7.5 mg/dL). Two CSM patients were on pre-operation, and one had a sequela, although it had been operated.

Although several medications have been reported to prolong the lifespan in murine ALS models, only a few clinical trials achieved good treatment outcomes [8,11,31]. One of the critical reasons for this discrepancy is the delay in clinical diagnosis [32]. According to the rEEC, diagnosis of ALS should be withheld until deterioration occurs in two or more affected regions and until several motor neurons are irreversibly damaged. In the present study, we found that cystatin C in the CSF could be a useful biomarker for the diagnosis of ALS in its early stages. Our subjects included eight patients who were diagnosed with possible and suspected ALS. We obtained CSF from these patients, and when their condition subsequently deteriorated, it was found to be similar to that occurring in ALS. The results of our present study may facilitate the early diagnosis of probable ALS before further progression to probable ALS. It is necessary to verify our results in a study with a larger sample size of patients and normal controls. Our samples were collected clinically; therefore, normal controls were absent. In two previous studies, the cystatin C concentration in the CSF was measured among normal controls and patients with minor neurological symptoms. These results showed a concentration of 5.8 ± 2.20 mg/L, which is 5.5 times greater than the concentration in plasma [14,17]. As compared to these studies, our data might indicate that cystatin C was upregulated in the case of polyneuropathy and the other disease controls. However, we consider that the concentration of cystatin C in ALS was reduced as reported in proteomics studies, while that in polyneuropathy and other diseases was near the normal range. This error may have resulted from the difference in the assay methods used, which should be eliminated in studies using larger sample sizes.

Cystatin C is an extracellular cysteine proteinase inhibitor that belongs to the cysteine superfamily [27]. It consists of 120 amino acids and is encoded by *CST3*, which has a leader sequence of 26 amino acids and is associated with the secreted protein. Cystatin C is expressed in various tissues [2], and it is present in all biological fluids. It is produced by the choroid plexus and secreted into the CSF, which contains the highest concentration of cystatin C as compared to the serum, urine, and saliva [1]. A missense mutation in the gene encoding cystatin C can lead to a hereditary human disease known as cerebral amyloid angiopathy (human cystatin C amyloid angiopathy, HCCAA) [24]. Pathological mutation of *L68Q* leads to the formation of dimers [4], whose conformational changes by three-dimensional domain swapping are amyloidogenic [15]. In this hereditary disease, there is abundant deposition of cystatin C along the vascular walls [22]. However, the concentration of cystatin C in the CSF is low [12]. Further, a cell line that expressed mutant cystatin C secreted it at lower levels than those of wild-type cystatin C; and the high levels of cystatin C aggregated within cells instead of being secreted from the cells [5]. This may imply that the mutation may have caused a breakdown in the protein transport mechanism. The deposition of Bunina bodies and the relatively low cystatin C concentration in the CSF in ALS patients might indicate that the mechanism underlying ALS may be similar to that of HCCAA.

Proteomics analysis of the CSF is a promising method for identifying biomarkers in neurological diseases. Thus far, alterations in several types of protein have been reported in various diseases. Alteration of cystatin C is found in several neurological disorders such as Creutzfeldt–Jakob disease [30], frontotemporal dementia [29], multiple sclerosis [20], and lumbar disk herniation [16]. However, recent articles have reported that cystatin C is truncated during storage at $-20\,^{\circ}C$ [10,13]. This information indicates that care should be taken during the storage and treatment of the samples containing cystatin C. Therefore, it is better to use fresh CSF aspirates when determining the levels of cystatin C to avoid an alteration in the concentration of this protein due to storage or treatment methods.

Analysis of CSF samples revealed that cystatin C can be used as a supplementary biomarker for the diagnosis of ALS in its early stages.

Acknowledgement

A grant from the Research Committee for ALS, the Ministry of Health, Labour and Welfare, Japan.

References

[1] M. Abrahamson, A.J. Barrett, G. Salvesen, A. Grubb, Isolation of six cysteine proteinase inhibitors from human urine. Their physicochemical and enzyme kinetic properties and concentrations in biological fluids, J. Biol. Chem. 261 (1986) 11282–11289.
[2] M. Abrahamson, I. Olafsson, A. Palsdottir, M. Ulvsback, A. Lundwall, O. Jensson, A. Grubb, Structure and expression of the human cystatin C gene, Biochem. J. 268 (1990) 287–294.
[3] E. Beghi, A. Millul, A. Micheli, E. Vitelli, G. Logroscino, SLALOM. Group, Incidence of ALS in Lombardy, Italy, Neurology 68 (2007) 141–145.
[4] M. Bjarnadottir, C. Nilsson, V. Lindström, A. Westman, P. Davidsson, F. Thormodsson, H. Blöndal, G. Gudmundsson, A. Grubb, The cerebral hemorrhage-producing cystatin C variant (L68Q) in extracellular fluids, Amyloid 8 (2001) 1–10.

[5] M. Bjarnadottir, B.S. Wulff, M. Sameni, B.F. Sloane, D. Keppler, A. Grubb, M. Abrahamson, Intracellular accumulation of the amyloidogenic L68Q variant of human cystatin C in NIH/3T3 cells, Mol. Pathol. 51 (1998) 317–326.
[6] B.R. Brooks, Diagnostic dilemmas in amyotrophic lateral sclerosis, J. Neurol. Sci. 165 (Suppl. 1) (1999) S1–S9.
[7] B.R. Brooks, R.G. Miller, M. Swash, T.L. Munsat, El Escorial revisited: revised criteria for the diagnosis of amyotrophic lateral sclerosis, Amyotroph. Lateral Scler. Motor Neuron Disord. 1 (2000) 293–299.
[8] M.E. Cudkowicz, J.M. Shefner, D.A. Schoenfeld, H. Zhang, K.I. Andreasson, J.D. Rothstein, D.B. Drachman, Trial of celecoxib in amyotrophic lateral sclerosis, Ann. Neurol. 60 (2006) 22–31.
[9] R. Davenport, R. Swingler, A. Chancellor, C. Warlow, Avoiding false positive diagnoses of motor neuron disease: lessons from the Scottish Motor Neuron Disease Register, J. Neurol. Neurosurg. Psychiatry 60 (1996) 147–151.
[10] P. Del Boccio, D. Pieragostino, A. Lugaresi, M. Di Ioia, B. Pavone, D. Travaglini, S. D'Aguanno, S. Bernardini, P. Sacchetta, G. Federici, C. Di Ilio, D. Gambi, A. Urbani, Cleavage of cystatin C is not associated with multiple sclerosis, Ann. Neurol. 62 (2007) 201–204, discussion 205.
[11] P.H. Gordon, D.H. Moore, R.G. Miller, J.M. Florence, J.L. Verheijde, C. Doorish, J.F. Hilton, G.M. Spitalny, R.B. MacArthur, H. Mitsumoto, H.E. Neville, K. Boylan, T. Mozaffar, J.M. Belsh, J. Ravits, R.S. Bedlack, M.C. Graves, L.F. McCluskey, R.J. Barohn, R. Tandan, Western ALS Study Group, Efficacy of minocycline in patients with amyotrophic lateral sclerosis: a phase III randomised trial, Lancet Neurol. 6 (2007) 1045–1053.
[12] A. Grubb, O. Jensson, G. Gudmundsson, A. Arnason, H. Lofberg, J. Malm, Abnormal metabolism of gamma-trace alkaline microprotein. The basic defect in hereditary cerebral hemorrhage with amyloidosis, N. Engl. J. Med. 311 (1984) 1547–1549.
[13] S.F. Hansson, A.H. Simonsen, H. Zetterberg, O. Andersen, S. Haghighi, I. Fagerberg, U. Andreasson, A. Westman-Brinkmalm, A. Wallin, U. Ruetschi, K. Blennow, Cystatin C in cerebrospinal fluid and multiple sclerosis, Ann. Neurol. 62 (2007) 193–196, discussion 205.
[14] H. Ishiguro, I. Ohkubo, M. Mizokami, K. Titani, M. Sasaki, The use of monoclonal antibodies to define levels of cystatin C in normal human serum, Hybridoma 8 (1989) 303–313.
[15] R. Janowski, M. Kozak, E. Jankowska, Z. Grzonka, A. Grubb, M. Abrahamson, M. Jaskolski, Human cystatin C, an amyloidogenic protein, dimerizes through three-dimensional domain swapping, Nat. Struct. Biol. 8 (2001) 316–320.
[16] X.D. Liu, B.F. Zeng, J.G. Xu, H.B. Zhu, Q.C. Xia, Proteomic analysis of the cerebrospinal fluid of patients with lumbar disk herniation, Proteomics 6 (2006) 1019–1028.
[17] H. Lofberg, A.O. Grubb, Quantitation of gamma-trace in human biological fluids: indications for production in the central nervous system, Scand. J. Clin. Lab. Invest. 39 (1979) 619–626.
[18] A.A. Makki, M. Benatar, The electromyographic diagnosis of amyotrophic lateral sclerosis: does the evidence support the El Escorial criteria? Muscle Nerve 35 (2007) 614–619.
[19] Y. Mizuno, M. Amari, M. Takatama, H. Aizawa, B. Mihara, K. Okamoto, Transferrin localizes in Bunina bodies in amyotrophic lateral sclerosis, Acta Neuropathol. 112 (2006) 597–603.
[20] I. Nakashima, M. Fujinoki, K. Fujihara, T. Kawamura, T. Nishimura, M. Nakamura, Y. Itoyama, Alteration of cystatin C in the cerebrospinal fluid of multiple sclerosis, Ann. Neurol. 62 (2007) 197–200, discussion 205.
[21] K. Okamoto, S. Hirai, M. Amari, M. Watanabe, A. Sakurai, Bunina bodies in amyotrophic lateral sclerosis immunostained with rabbit anti-cystatin C serum, Neurosci. Lett. 162 (1993) 125–128.
[22] I. Olafsson, L. Thorsteinsson, O. Jensson, The molecular pathology of hereditary cystatin C amyloid angiopathy causing brain hemorrhage, Brain Pathol. 6 (1996) 121–126.
[23] O. O'Toole, B.J. Traynor, P. Brennnan, C. Sheehan, E. Frost, B. Corr, O. Hardiman, Epidemiology and clinical features of amyotrophic lateral sclerosis in Ireland between 1995 and 2004, J. Neurol. Neurosurg. Psychiatry 79 (2008) 30–32.
[24] A. Palsdottir, M. Abrahamson, L. Thorsteinsson, A. Arnason, I. Olafsson, A. Grubb, O. Jensson, Mutation in cystatin C gene causes hereditary brain haemorrhage, Lancet 2 (1988) 603–604.
[25] G.M. Pasinetti, L.H. Ungar, D.J. Lange, S. Yemul, H. Deng, X. Yuan, R.H. Brown, M.E. Cudkowicz, K. Newhall, E. Peskind, S. Marcus, L. Ho, Identification of potential CSF biomarkers in ALS, Neurology 66 (2006) 1218–1222.
[26] S. Ranganathan, E. Williams, P. Ganchev, V. Gopalakrishnan, D. Lacomis, L. Urbinelli, K. Newhall, M.E. Cudkowicz, R.H. Brown Jr., R. Bowser, Proteomic profiling of cerebrospinal fluid identifies biomarkers for amyotrophic lateral sclerosis, J. Neurochem. 95 (2005) 1461–1471.
[27] C.H. Reed, Diagnostic applications of cystatin C, Br. J. Biomed. Sci. 57 (2000) 323–329.
[28] D.R. Rosen, T. Siddique, D. Patterson, D.A. Figlewicz, P. Sapp, A. Hentati, D. Donaldson, J. Goto, J.P. O'Regan, H.X. Deng, Z. Rahmani, A. Krizus, D. McKenna-Yasek, A. Cayabyab, S.M. Gaston, R. Berger, R.E. Tanzi, J.J. Halperin, B. Herzfeldt, R. Van den Bergh, W.Y. Hung, T. Bird, G. Deng, D.W. Mulder, C. Smyth, N.G. Laing, E. Soriano, M.A. Pericak-Vance, J. Haines, G.A. Rouleau, J.S. Gusella, H.R. Horvitz, R.H. Brown, Mutations in Cu/Zn superoxide dismutase gene are associated with familial amyotrophic lateral sclerosis, Nature 362 (1993) 59–62.
[29] U. Ruetschi, H. Zetterberg, V.N. Podust, J. Gottfries, S. Li, A. Hviid Simonsen, J. McGuire, M. Karlsson, L. Rymo, H. Davies, L. Minthon, K. Blennow, Identification of CSF biomarkers for frontotemporal dementia using SELDI-TOF, Exp. Neurol. 196 (2005) 273–281.
[30] J.C. Sanchez, E. Guillaume, P. Lescuyer, L. Allard, O. Carrette, A. Scherl, J. Burgess, G.L. Corthals, P.R. Burkhard, D.F. Hochstrasser, Cystatin C as a potential cerebrospinal fluid marker for the diagnosis of Creutzfeldt–Jakob disease, Proteomics 4 (2004) 2229–2233.
[31] J.M. Shefner, M.E. Cudkowicz, D. Schoenfeld, T. Conrad, J. Taft, M. Chilton, L. Urbinelli, M. Qureshi, H. Zhang, A. Pestronk, J. Caress, P. Donofrio, E. Sorenson, W. Bradley, C. Lomen-Hoerth, E. Pioro, K. Rezania, M. Ross, R. Pascuzzi, T. Heiman-Patterson, R. Tandan, H. Mitsumoto, J. Rothstein, T. Smith-Palmer, D. MacDonald, D. Burke, NEALS Consortium, A clinical trial of creatine in ALS, Neurology 63 (2004) 1656–1661.
[32] M. Swash, Learning from failed trials in ALS, Lancet Neurol. 6 (2007) 1034–1035.
[33] B.J. Traynor, M.B. Codd, B. Corr, C. Forde, E. Frost, O. Hardiman, Amyotrophic lateral sclerosis mimic syndromes: a population-based study, Arch. Neurol. 57 (2000) 109–113.
[34] B.J. Traynor, M.B. Codd, B. Corr, C. Forde, E. Frost, O.M. Hardiman, Clinical features of amyotrophic lateral sclerosis according to the El Escorial and Airlie House diagnostic criteria: a population-based study, Arch. Neurol. 57 (2000) 1171–1176.
[35] K. Wakabayashi, M. Yoshimoto, S. Tsuji, H. Takahashi, Alpha-synuclein immunoreactivity in glial cytoplasmic inclusions in multiple system atrophy, Neurosci. Lett. 249 (1998) 180–182.
[36] S. Zoccolella, E. Beghi, G. Palagano, A. Fraddosio, V. Samarelli, P. Lamberti, V. Lepore, L. Serlenga, G. Logroscino, SLAP registry, signs and symptoms at diagnosis of amyotrophic lateral sclerosis: a population-based study in southern Italy, Eur. J. Neurol. 13 (2006) 789–792.

Neurobiology of Disease

Neuroaxonal Dystrophy Caused by Group VIA Phospholipase A_2 Deficiency in Mice: A Model of Human Neurodegenerative Disease

Koei Shinzawa,[1] Hisae Sumi,[2] Masahito Ikawa,[3] Yosuke Matsuoka,[1] Masaru Okabe,[3] Saburo Sakoda,[2] and Yoshihide Tsujimoto[1]

[1]Department of Medical Genetics, Laboratory of Molecular Genetics and Solution-Oriented Research for Science and Technology, Japan Science and Technology Agency, and [2]Department of Neurology, Osaka University Medical School, Osaka 565-0871, Japan, and [3]Research Institute for Microbial Diseases, Osaka University, Osaka 565-0871, Japan

Calcium-independent group VIA phospholipase A_2 (iPLA$_2\beta$) is considered to play a role in signal transduction and maintenance of homeostasis or remodeling of membrane phospholipids. A role of iPLA$_2\beta$ has been suggested in various physiological and pathological processes, including immunity, chemotaxis, and cell death, but the details remain unclear. Accordingly, we investigated mice with targeted disruption of the *iPLA$_2\beta$* gene. *iPLA$_2\beta^{-/-}$* mice developed normally and grew to maturity, but all showed evidence of severe motor dysfunction, including a hindlimb clasping reflex during tail suspension, abnormal gait, and poor performance in the hanging wire grip test. Neuropathological examination of the nervous system revealed widespread degeneration of axons and/or synapses, accompanied by the presence of numerous spheroids (swollen axons) and vacuoles. These findings provide evidence that impairment of *iPLA$_2\beta$* causes neuroaxonal degeneration, and indicate that the *iPLA$_2\beta^{-/-}$* mouse is an appropriate animal model of human neurodegenerative diseases associated with mutations of the *iPLA$_2\beta$* gene, such as infantile neuroaxonal dystrophy and neurodegeneration with brain iron accumulation.

Key words: **phospholipase; neurodegeneration; neuroaxonal dystrophy; knock-out mouse; iPLA$_2$; spheroid**

Introduction

The phospholipases A_2 (PLA$_2$) comprise a family of esterases that hydrolyze the *sn-2* ester bond in phospholipids to yield free fatty acids and lysophospholipids. A number of PLA$_2$ isotypes have been identified in mammals, and depending on their subcellular localization and enzymatic properties, these are divided into three major subfamilies, which are secretory PLA$_2$ (sPLA$_2$), cytosolic Ca^{2+}-dependent PLA$_2$ (cPLA$_2$), and Ca^{2+}-independent PLA$_2$ (iPLA$_2$) (Six and Dennis, 2000; Ma and Turk, 2001). The sPLA$_2$s are extracellular enzymes with a low molecular mass (~14 kDa) that require millimolar concentrations of Ca^{2+} for activation. sPLA$_2$s are thought to be potent mediators of inflammation and also show antibacterial activity. In contrast, the cPLA$_2$s are intracellular enzymes that specifically target arachidonic acid at the *sn-2* position of phospholipids. Their activity is regulated by submicromolar levels of Ca^{2+}, and these enzymes are believed to play a pivotal role in the production of arachidonic acid metabolites, such as eicosanoids. The iPLA$_2$s do not require Ca^{2+} for their catalytic activity and are suggested to be involved in remodeling of membrane phospholipids as well as in various cellular signaling processes. In mammals, two iPLA$_2$ genes (iPLA$_2\beta$ and iPLA$_2\gamma$) have been cloned (Tang et al., 1997; Mancuso et al., 2000).

The physiological role of the PLA$_2$s in the nervous system remains largely unknown in mammals. To our knowledge, there have been no previous reports about neurological dysfunction in PLA$_2$ knock-out mice. The *iPLA$_2\beta$* gene is expressed in all regions of the mammalian brain and iPLA$_2$ is the dominant PLA$_2$ activity in rat brain cytosol (Yang et al., 1999; Balboa et al., 2002). Accumulated evidence suggests that changes of phospholipids may be to associated with cell death, including apoptosis and necrosis (caspase-independent cell death) (Shinzawa and Tsujimoto, 2003), and may cause many neurodegenerative diseases, including cerebral infarction and Alzheimer disease (Farooqui et al., 2004). Moreover, it was very recently reported that *iPLA$_2\beta$* gene mutations occur in several human neurodegenerative disorders, such as infantile neuraxonal dystrophy (INAD) and neurodegeneration with brain iron accumulation (NBIA) (Khateeb et al., 2006; Morgan et al., 2006), which are all pathologically characterized by widespread development of axonal swellings (spheroids) in the central and peripheral nervous systems, suggesting that

Received Nov. 22, 2006; revised Jan. 15, 2008; accepted Jan. 17, 2008.

This work was supported in part by a grant from the 21st Century Center of Excellence Program, a Scientific Research grant from the Japanese Ministry of Education, Science, Sports, and Culture, and a Comprehensive Research on Aging and Health grant from the Ministry of Health, Labor and Welfare, Japan. We are grateful to Y. Maruyama, A. Kawai, T. Aikawa, K. Ideguchi, and Y. Haseda for technical assistance and Drs. S. Kato and M. Etoh for their helpful advice.

Correspondence should be addressed to Yoshihide Tsujimoto, Laboratory of Molecular Genetics, Osaka University Medical School, Room B8, 2-2 Yamadaoka, Suita, Osaka 565-0871, Japan. E-mail: tsujimot@gene.med.osaka-u.ac.jp.

DOI:10.1523/JNEUROSCI.4354-07.2008

 0270-6474/08/282212-09$15.00/0

impairment of *iPLA$_2\beta$* is involved in the pathogenesis of neuroaxonal dystrophy.

To explore the physiological and pathological role of *iPLA$_2\beta$*, we generated *iPLA$_2\beta^{-/-}$* mice. Here, we report that *iPLA$_2\beta^{-/-}$* mice developed motor dysfunction associated with prominent formation of spheroids and vacuoles in axons and synapses throughout the nervous system. These findings provide evidence that impairment of *iPLA$_2\beta$* causes neuroaxonal dystrophy.

Materials and Methods

Animal. The C57BL/6 mice used in this study were obtained from Japan SLC (Shizuoka, Japan). The experimental protocol was approved by the Ethical Review Committee for Animal Experimentation of Osaka University Medical School.

In situ *hybridization.* An RNA probe was prepared by *in vitro* transcription, as described previously (Matsuoka et al., 2002), using digoxigenin (DIG)-UTP and the pGEM-T easy plasmid vector (Promega, Madison, WI) carrying 720 bases (1732–2452) of mouse iPLA$_2\beta$ cDNA.

Brains, spinal cords, and dorsal root ganglia of the mice were dissected, submerged in OCT Tissue-Tek mounting medium (Miles, Elkhart, IN), and rapidly frozen at −40°C in 2-methyl-butane. Sections 7 μm thick were cut on a cryostat and mounted on Matsunami adhesive silane-coated slides (Matsunami, Osaka, Japan). Refixation, acetylation, and hybridization of the sections were performed as described previously (Zhong et al., 2004). After washing three times with 50% formamide and 2× SSC at 60°C, the sections were treated with blocking reagent for 30 min at room temperature, and then incubated with alkaline phosphatase-conjugated anti-DIG antibody for 30 min. After washing three times, the sections were incubated in 100 mM Tris-HCl, pH 9.5, 100 mM NaCl, 0.03% nitro blue tetrazolium, and 0.015% bromochloroindoyl phosphate. Then, color development was stopped by incubation in PBS containing 10 mM EDTA, after which the sections were treated in 100% ethanol and xylene, and then embedded for microscopic observation.

Targeted disruption of the iPLA$_2\beta$ *gene.* A vector for disruption of the *iPLA$_2\beta$* gene was constructed using genomic DNA derived from 129/Sv embryonic stem (ES) cells and the pMulti-ND-1.0 vector (Inoue et al., 2005). Briefly, a 2.3 kb genomic fragment containing exon 10 and a 7.7 kb genomic fragment containing exons 5–8 were inserted into the *Pac*I site and the *Cla*I site of the vector, respectively.

ES cells [clone D3 (p13GIRC)] were transfected with the vector, and neomycin-resistant clones were isolated. After screening 288 resistant clones by PCR and subsequently by Southern blot analysis of *Bgl*II-digested genomic DNA using a probe A or a probe B, two ES cells lines with disruption of the *iPLA$_2\beta$* gene were obtained. These ES cells were injected into C57BL/6 blastocysts to produce chimeric mice, which were crossed with C57BL/6 mice to obtain *iPLA$_2\beta^{+/-}$* F1 progeny. The littermates obtained from pairing of *iPLA$_2\beta^{+/-}$* F2 mice were pooled and used for this study.

Genotyping of mice by PCR and Southern blot analysis. Genomic DNA was prepared from mouse tails. To amplify the wild-type and disrupted *iPLA$_2\beta$* loci, the following primers were used: wild-type (349 bp), ATGGATCCGTGGTCTTCATCTACCTCCTCG and TGAGCCCAATGCTAGGAATGTCCAATCAGC; disrupted *iPLA$_2\beta$* locus (480 bp), TGGCGGACCGCTATCAGGACATAGCGTTGG and AGGTGGAGTGCAGGAACAAGGCCTATCAGG.

The PCR was performed using a Gene *Taq* (Nippon Gene, Tokyo, Japan), with 32 cycles of 95°C for 30 s, 63°C for 30 s, and 72°C for 1 min. Southern blot analysis was performed using a Gene Images kit (GE Healthcare Bio-Science, Piscataway, NJ). The probes were prepared by PCR using a dNTP mixture containing fluorescein-11-dUTP and the following primes: probe A (423 bp), GCCGGCCTGAACCAGGTAAACAACCAAGGG and TGACCTGCCAAGCAGCAGACTCAAGAGCAG; probe B (777 bp), TCAAGAAGGCGATAGAAGGCGATGCGCTGC and TGAACAAGATGGATTGCACGCAGGTTCTCC. Hybridization, washing, and detection were performed according to the supplier's protocol.

Western blot analysis. Testes obtained from male mice were homogenized with radioimmunoprecipitation assay buffer (50 mM Tris-HCl, pH 7.4, 150 mM NaCl, 1% Nonidet P-40, 0.5% sodium deoxycholate, 0.1% SDS, and protease inhibitor mixture). As described previously (Shinzawa and Tsujimoto, 2003), immunoblot analysis was performed with a polyclonal anti-iPLA$_2\beta$ antibody (Cayman Chemical, Ann Arbor, MI) or a monoclonal anti-α-tubulin antibody (clone B-5-1-2) (Sigma, St. Louis, MO) and an HRP-conjugated secondary antibody using ECL Western blotting detection reagents (GE Healthcare Bio-Science).

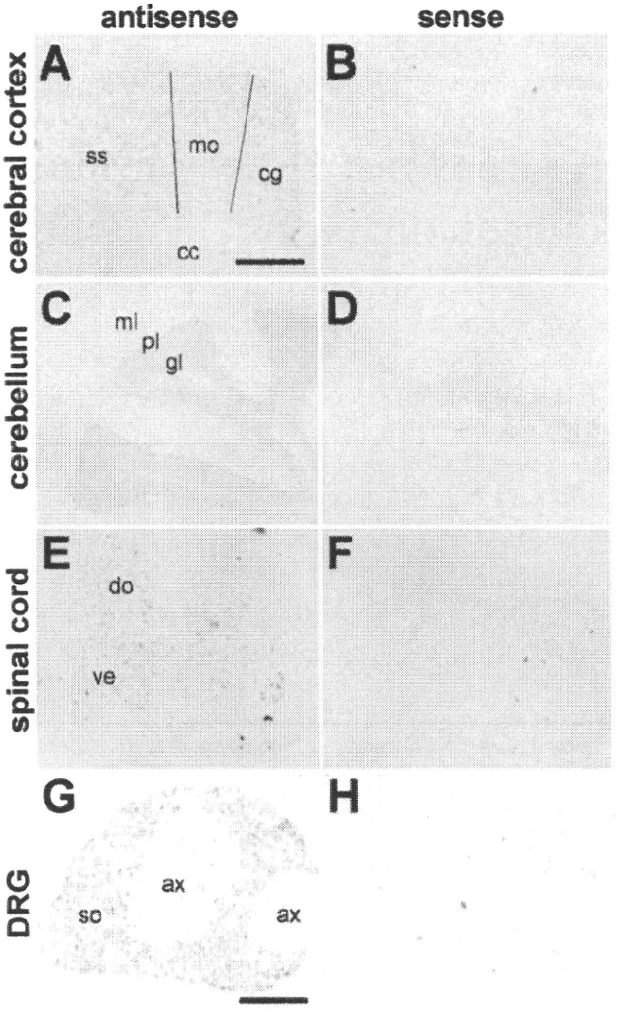

Figure 1. *In situ* hybridization of iPLA$_2\beta$ mRNA in the nervous system. ***A–H***, The pattern of iPLA$_2\beta$ mRNA expression in the cerebral cortex (***A***, ***B***), the cerebellum (***C***, ***D***), the spinal cord (***E***, ***F***), and the dorsal root ganglion (DRG) (***G***, ***H***) of 7-week-old female mice. The antisense probe detected signals in all cortical layers, except for layer I, of the cingulate (cg), the motor (mo) cortex, and the somatosensory (ss) cortex, in the Purkinje cell layer (pl) and the granular layer (gl), but not the molecular layer (ml) of the cerebellum, in the dorsal (do) and ventral (ve) horns of the spinal cord, and the soma-rich region of the DRG (so). No signals were detected in the corpus callosum (cc) or in the axon-rich region (ax) that contains mainly axons and oligodendrocytes (cc) or Schwann cells (ax). The sense probe was used as a negative control (***B***, ***D***, ***F***, ***H***). Scale bars: ***A–F***, 500 μm; ***G***, ***H***, 180 μm.

Behavioral analysis. The hanging wire grip test was performed by placing a mouse on a wire net and then turning the net upside down at a height of ~20 cm above the cage floor to prevent the animal from easily climbing down. The time that elapsed until the animal fell was recorded three times and the cutoff time was set at 60 s. Footprint patterns were obtained by painting the forepaws and the hindpaws with blue and red ink, respectively.

Histochemical and immunohistochemical analysis. Mice aged 95–103 weeks (*iPLA$_2\beta^{+/+}$*, one male and three females; and *iPLA$_2\beta^{-/-}$*, three males and four females), mice aged 56 weeks (*iPLA$_2\beta^{+/+}$*, one female;

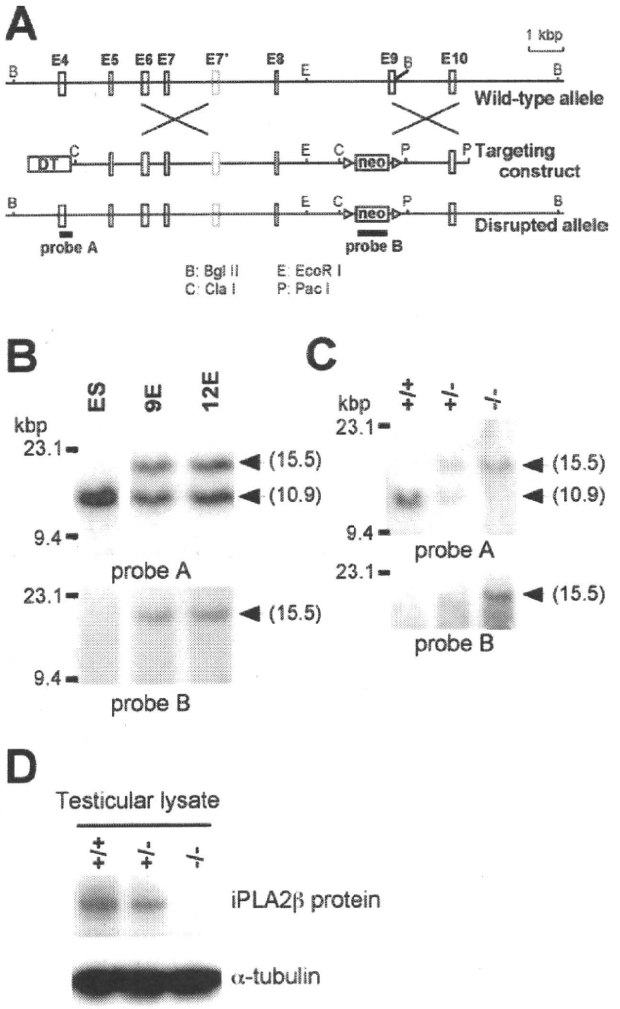

Figure 2. Targeting the *iPLA$_2\beta$* gene. ***A***, Diagram of the wild-type *iPLA$_2\beta$* gene, the targeting construct, and the disrupted *iPLA$_2\beta$* allele. ***B***, ***C***, Southern blot analysis of *Bgl*II-digested genomic DNA from ES cell clones (***B***) and from the tails of *iPLA$_2\beta^{+/+}$*, *iPLA$_2\beta^{+/-}$*, and *iPLA$_2\beta^{-/-}$* mice (***C***). The DNA probes used for Southern blot analysis were a probe A and B containing exon 4 and neomycin resistance gene (neo), respectively. The *iPLA$_2\beta^{+/+}$* wild-type allele generated a band of 10.9 kbp, whereas the disrupted allele yielded a 15.5 kbp fragment. ***D***, Western blotting of testicular lysates with an anti-iPLA$_2\beta$ antibody (α-tubulin was used as the loading control).

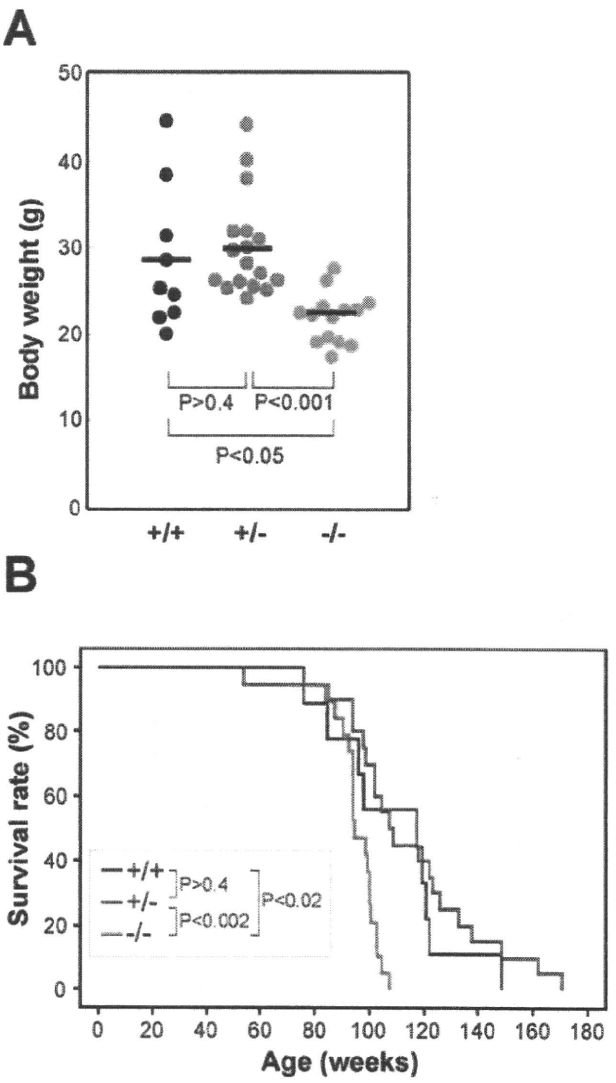

Figure 3. Lower body weight and shorter lifespan of *iPLA$_2\beta^{-/-}$* mice. ***A***, Body weight of female *iPLA$_2\beta^{+/+}$* mice ($n = 9$), *iPLA$_2\beta^{+/-}$* mice ($n = 17$), and *iPLA$_2\beta^{-/-}$* mice ($n = 14$) at 91–100 weeks of age. Bars indicate the mean values. p values were calculated using the Student's t test. ***B***, Survival of female *iPLA$_2\beta^{+/+}$* mice ($n = 9$), *iPLA$_2\beta^{+/-}$* mice ($n = 20$), and *iPLA$_2\beta^{-/-}$* mice ($n = 19$). p values were calculated using the log-rank test. Results obtained with male mice were virtually identical.

and *iPLA$_2\beta^{-/-}$*, four females), mouse aged 32 weeks (*iPLA$_2\beta^{-/-}$*, one female), and mice aged 15 weeks (*iPLA$_2\beta^{-/-}$*, one male and one female) were used for histological examination. After being treated with an overdose of sodium pentobarbital, each animal was perfused with PBS and then 4% paraformaldehyde. The brain, spinal cord, and sciatic nerve were removed from each mouse, immersed in the same fixative overnight at 4°C, and then dehydrated and embedded in paraffin blocks. Then 4-μm-thick paraffin sections were prepared and stained with hematoxylin and eosin (H&E), Nissl, Luxol fast blue, periodic acid-Shiff (PAS), Bielschowsky, or Berlin blue stain. Small pieces of sciatic nerves from mice aged 95–103 weeks and the cerebral cortex and the dorsal part of the cervical spinal cord from mice aged 56 weeks were fixed with 2.5% glutaraldehyde and processed to Epon blocks as described previously (Sumi et al., 2006). Transverse Epon sections, 1 μm thick, of sciatic nerves were stained with toluidine blue.

To perform immunohistochemistry, deparaffinized sections were processed as described previously (Sumi et al., 2006). The antibodies used were a mouse monoclonal antibody for phosphorylated neurofilament (Covance, Berkeley, CA) and rabbit polyclonal antibody for ubiquitin (Dako, Glostrup, Denmark). Hematoxylin was used to counterstain the cell nuclei.

To estimate the total density of myelinated nerve fibers in the sciatic nerve per unit area, three images of the large nerve fascicles (100× objective, 62,080 μm^2) were obtained with a digital camera (VB-7010; Keyence, Osaka, Japan) attached to a light microscope (Eclipse E800; Nikon, Tokyo, Japan), and the number of myelinated fibers in the four images was counted in each mouse. To estimate the area of the sciatic nerves, images of the whole nerve (10× objective) were obtained with a digital camera attached to the light microscope, and the areas of all nerve fascicles were measured using image analysis software (VH-H1A5; Keyence). The total number of myelinated fibers in the sciatic nerve was calculated from the density and the area.

Ultrathin sections of the cerebral cortex and the dorsal horn were cut and stained with uranyl acetate and lead citrate, and were examined by transmission electron microscopy (H-7650; Hitachi, Tokyo, Japan).

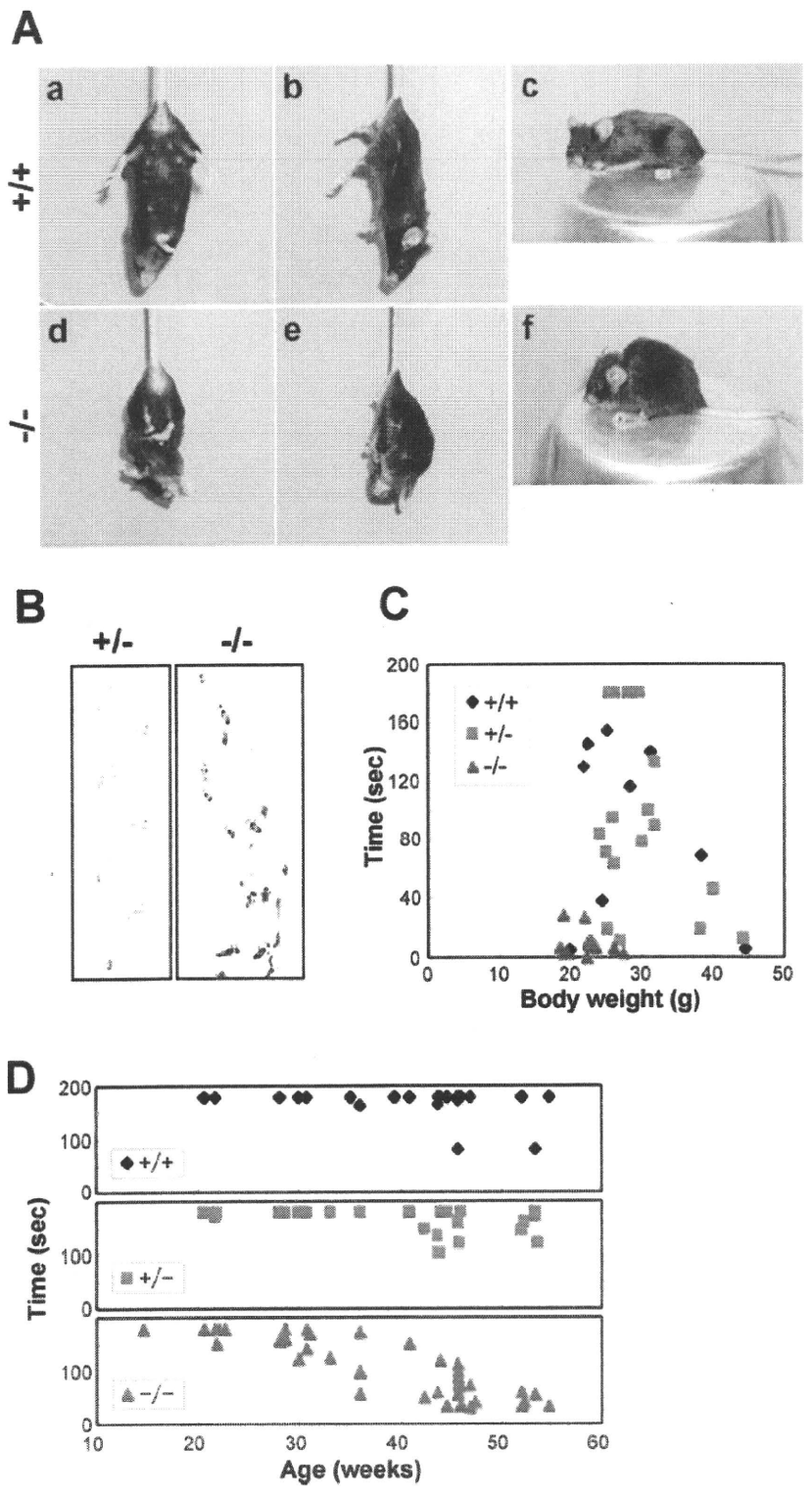

Figure 4. Motor dysfunction in $iPLA_2\beta^{-/-}$ mice. ***A***, Representative photographs of an $iPLA_2\beta^{+/+}$ mouse (***a–c***) and an $iPLA_2\beta^{-/-}$ mouse (***d–f***) at 95 weeks of age. The $iPLA_2\beta^{-/-}$ mouse adopts a feet-clasping posture when suspended by the tail (***d***, ***e***), whereas the $iPLA_2\beta^{+/+}$ mouse holds its hindlimbs outward to steady itself (***a***, ***b***). The $iPLA_2\beta^{-/-}$ mouse has a hunched posture (***f***). ***B***, Representative footprint patterns of $iPLA_2\beta^{+/-}$ and $iPLA_2\beta^{-/-}$ mice at 90 and 87 weeks of age, respectively. Forepaws and hindpaws were painted with blue and red ink, respectively. The $iPLA_2\beta^{-/-}$ mouse displays an irregular stride and dragging of the hindlimbs. ***C***, ***D***, Hanging wire grip test. ***C***, Female $iPLA_2\beta^{+/+}$ mice ($n = 9$), $iPLA_2\beta^{+/-}$ mice ($n = 17$), and $iPLA_2\beta^{-/-}$ mice ($n = 13$) (91–100 weeks old) were tested as described in Materials and Methods, and the total time for three trials was plotted against body weight. ***D***, Female $iPLA_2\beta^{+/+}$ mice ($n = 23$), $iPLA_2\beta^{+/-}$ mice ($n = 25$), and $iPLA_2\beta^{-/-}$ mice ($n = 42$) (15–55 weeks old) were tested. The total time for three trials was plotted against age.

Results

Expression of $iPLA_2\beta$ mRNA in the nervous system

As described below, $iPLA_2\beta^{-/-}$ mice suffered from neurodegeneration. Accordingly, we performed detailed examination of the pattern of $iPLA_2\beta$ gene expression in the nervous system by *in situ* hybridization. Because of unavailability of suitable anti-iPLA$_2\beta$ antibody, we were unable to perform immunohistochemical analysis. As shown in Figure 1*A*, every layer of the cerebral cortex, except for layer I, was stained by the antisense probe for the $iPLA_2\beta$ gene, but not by the sense probe (Fig. 1*B*). No signals were detected in the corpus callosum where axons and oligodendrocytes are prominent. In the cerebellum, weak $iPLA_2\beta$ gene expression was seen in the granular layer, whereas there was stronger expression in the Purkinje cells (Fig. 1*C*). In the spinal cord, both dorsal and ventral horn neurons showed strong expression of the $iPLA_2\beta$ gene (Fig. 1*E*). Moreover, dorsal root ganglion cells showed somatic expression of $iPLA_2\beta$, although there was no expression in their axons or in the Schwann cells (Fig. 1*G*). Together, these results indicated that the $iPLA_2\beta$ gene was widely expressed by neurons.

Generation of $iPLA_2\beta^{-/-}$ mice

To evaluate the physiological role of $iPLA_2\beta$, we generated mice with targeted disruption of the $iPLA_2\beta$ gene. As described in Figure 2*A*, a targeting vector was designed, so that exon 9 (which encodes the catalytic domain including the active center amino acid residue, Ser 465) was replaced by a neomycin resistance gene (neo) cassette. Following the standard procedure described in Materials and Methods, two ES cell lines (9E and 12E) with the disrupted allele were obtained (Fig. 2*B*) and then injected into blastocysts to produce chimeric mice. One of the two cell lines (9E) transmitted the disrupted allele to the germline. $iPLA_2\beta^{+/-}$ mice were interbred to generate $iPLA_2\beta^{-/-}$ mice and their offspring were genotyped by PCR and Southern blot analysis (Fig. 2*C*). The absence of iPLA$_2\beta$ protein in $iPLA_2\beta^{-/-}$ mice was confirmed by Western blot analysis using testicular lysates (Fig. 2*D*), indicating that the disrupted allele was a null mutation. The ratio of offspring with each genotype was in accordance with the Mendelian rule ($iPLA_2\beta^{+/+}$:$iPLA_2\beta^{+/-}$:$iPLA_2\beta^{-/-}$ = 81:141:67). $iPLA_2\beta^{-/-}$ mice developed normally and grew to maturity. Male mice exhibited reduced fertility (data

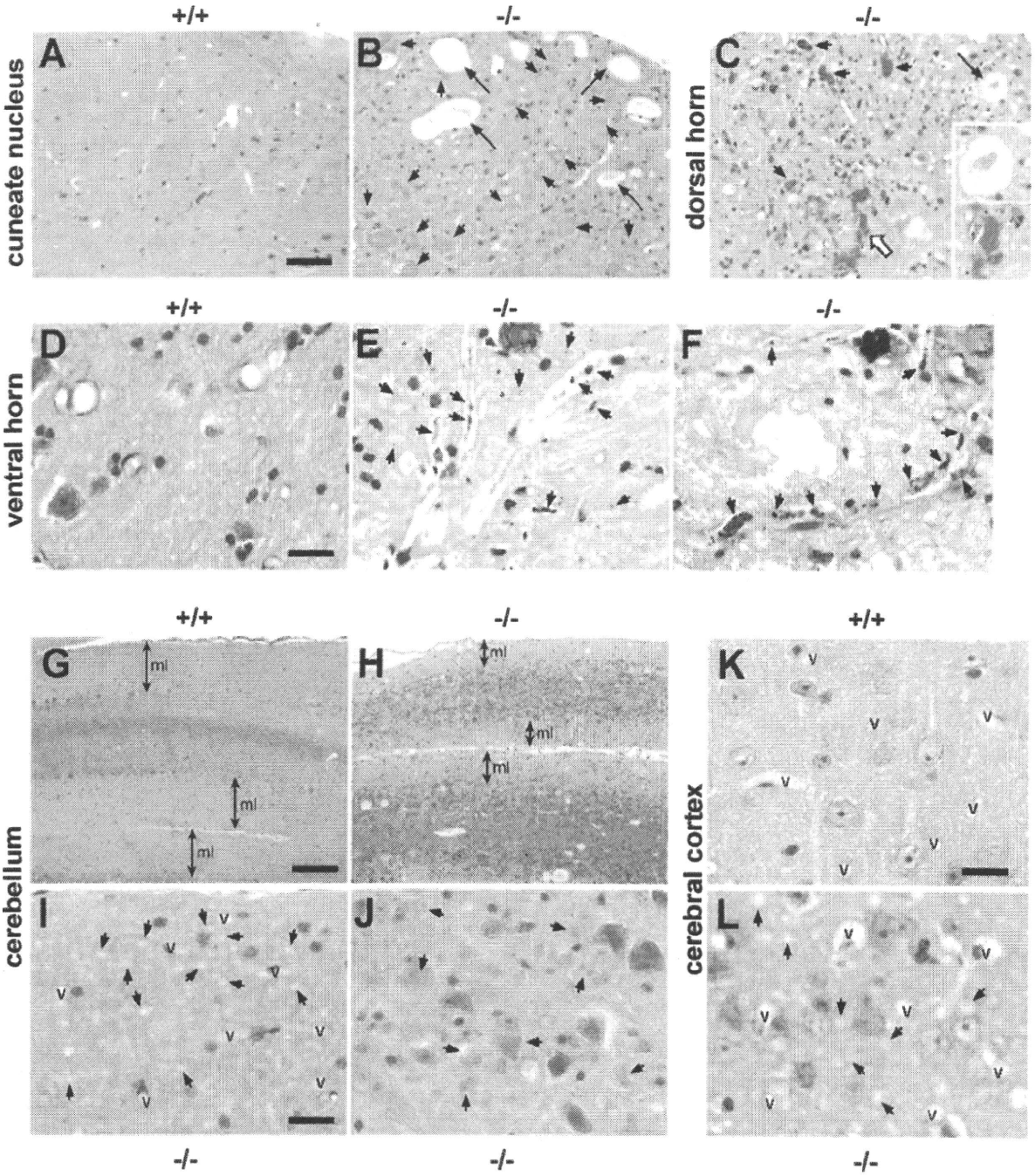

Figure 5. Neuropathological changes in $iPLA_2\beta^{-/-}$ mice. ***A***, ***B***, Cuneate nucleus of an $iPLA_2\beta^{+/+}$ mouse (***A***) and an $iPLA_2\beta^{-/-}$ mouse (***B***) at 2 years (95–103 weeks old). ***C***, Dorsal horn of $iPLA_2\beta^{-/-}$ mouse at 2 years. ***D–F***, Ventral horn of an $iPLA_2\beta^{+/+}$ mouse at 56 weeks (***D***) and an $iPLA_2\beta^{-/-}$ mouse at 15 weeks (***E***) and 2 years (***F***). ***G***, ***H***, Cerebellum of an $iPLA_2\beta^{+/+}$ mouse (***G***) and an $iPLA_2\beta^{-/-}$ mouse (***H***) at 2 years. ***I***, ***J***, Molecular layer (***I***) and dentate nucleus (***J***) of the cerebellum of an $iPLA_2\beta^{-/-}$ mouse at 15 weeks. ***K***, ***L***, Cerebral cortex of an $iPLA_2\beta^{+/+}$ mouse (***K***) and an $iPLA_2\beta^{-/-}$ mouse (***L***) at 2 years. ***A***, ***B***, ***G–L***, H&E stain. ***C–F***, PAS stain. ***A***, No spheroids and vacuoles are detected in the $iPLA_2\beta^{+/+}$ mouse. ***B***, Many spheroids (arrows) and large vacuoles (large arrows) can be observed. ***C***, Irregular PAS-positive spheroids (small arrows) contain fissures, vacuoles, and PAS-positive granules. The extent of PAS staining is variable. The core of the huge vacuole contains PAS-positive granules (large arrow and open arrow; also shown at a higher magnification). ***D***, No PAS-positive granules are observed in the $iPLA_2\beta^{+/+}$ mouse. ***E***, Strongly PAS-positive granules can be seen in normal-looking axons or the neuropil. ***F***, PAS-positive granules (arrows) in swollen axons. ***G***, ***H***, The molecular layer (ml) of the cerebellum from the $iPLA_2\beta^{-/-}$ mouse (***H***) is thinner than that from the $iPLA_2\beta^{+/+}$ mouse (***G***). ***I***, Numerous tiny vacuoles (arrows) can be seen in the molecular layer. ***J***, There are only a few spheroids (arrows). ***K***, There are no detectable vacuoles in the $iPLA_2\beta^{+/+}$ mouse. ***L***, Numerous small vacuoles (arrows) can be observed, but there are no spheroids. Scale bars: ***A–C***, 50 μm; ***D–F***, ***I–L***, 16 μm; ***G***, ***H***, 100 μm. v, Vessels.

not shown), confirming previous observations (Bao et al., 2004).

Neurodegeneration and shortened lifespan

Because we could not find any obvious abnormalities of $iPLA_2\beta^{-/-}$ mice by the age of 1 year, except for reduced fertility in males, a substantial number of mice were kept alive to examine the effect on their lifespan and aging. Although at 40–50 weeks no difference of body weight between $iPLA_2\beta^{-/-}$ mice and their littermates (supplemental Fig. 1*A*, available at www.jneurosci.org as supplemental material), $iPLA_2\beta^{-/-}$ mice gradually lost weight and died earlier than their littermates (Fig. 3*A*,*B*). The

Table 1. Distribution of spheroids and vacuoles in the CNS

Region	Spheroids	Vacuoles
Cuneate nucleus	+++	++
Gracile nucleus	+++	++
Trigeminal nucleus	+++	++
Facial nucleus	++	+
Cochlear nucleus	+++	++
Vestibular nucleus	+++	++
Hypoglossal nucleus	+	+
Spinal cord		
dorsal horn	+++	++
ventral horn	++	++
dorsal funiculus	++	++
ventral funiculus	++	++
Striatum	+	++
Thalamus	+	++
Hypothalamus	+	++
Hippocampus	+	++ (small)[a]
Amygdala	+	++
Cerebellum		
molecular layer	+	++ (small)[a]
granular layer	+	++
dentate nucleus	++	++
Cerebral cortex	+/−	+++ (small)[a]

Distribution of spheroids and vacuoles in the CNS were assessed and graded as follows: +/−, very few; +, mild degree; ++, moderate degree; +++, marked degree.

[a]Vacuoles of small size were predominantly observed. Mice aged 95–103 weeks were examined.

log-rank test indicated there was a significant survival difference between $iPLA_2\beta^{-/-}$ and $iPLA_2\beta^{+/+}$ mice ($p < 0.02$), and between $iPLA_2\beta^{-/-}$ and $iPLA_2\beta^{+/-}$ mice ($p < 0.002$). The median lifespan of $iPLA_2\beta^{-/-}$ mice was 90 weeks compared with 110–115 weeks for their littermates. By the age of 2 years, all of the $iPLA_2\beta^{-/-}$ mice showed abnormal movement of their hindlimbs. When held by the tail, $iPLA_2\beta^{-/-}$ mice moved their hindlimbs randomly in all directions or stopped moving with feet clasping, and a dangling posture being prominent (Fig. 4*Ad*,*Ae*). The mice seemed unable to use their hindlimbs to maintain their balance as they tried to raise their heads. In contrast, $iPLA_2\beta^{+/+}$ mice extended their hindlimbs out from the trunk to maintain their balance (Fig. 4*Aa*,*Ab*), and could easily raise their heads. Moreover, $iPLA_2\beta^{-/-}$ mice dragged their hindlimbs when walking and had an irregular stride (Fig. 4*B*). In contrast, $iPLA_2\beta^{+/+}$ and $iPLA_2\beta^{+/-}$ mice did not show any of these changes. When motor function was assessed by the hanging wire grip test, the mice were placed on a wire net that was turned upside down, and the time until the animal fell was recorded three times. Because body weight was predicted to affect the time until falling, the weight was plotted against time (Fig. 4*C*). All of the $iPLA_2\beta^{-/-}$ mice showed impaired motor function in this test. The $iPLA_2\beta^{-/-}$ mice also tended to adopt a hunched posture (Fig. 4*Af*), although x-ray radiograms did not reveal any obvious differences of bone structure or density (data not shown). After analysis of 2-year-old mice, the behavioral abnormalities of younger $iPLA_2\beta^{-/-}$ mice (≤1 year old) were carefully monitored. Although $iPLA_2\beta^{-/-}$ mice did not show obvious abnormalities in the footprint and tail suspension tests by the age of 55 weeks (supplemental Fig. 1*B*, available at www.jneurosci.org as supplemental material) (data not shown), the hanging wire grip test was definitely abnormal. Their time scores decreased gradually from the age of 30 weeks, and by the age of ~50 weeks all of the $iPLA_2\beta^{-/-}$ mice showed very low time scores (Fig. 4*D*). These results indicate that the hanging wire grip test may be more sensitive for detecting impaired motor function in $iPLA_2\beta^{-/-}$ mice. All together, these findings indicated that iPLA$_2\beta$ deficiency led to the onset of motor dysfunction and a shorter lifespan.

Neuropathological findings in $iPLA_2\beta^{-/-}$ mice

The $iPLA_2\beta^{-/-}$ mice were subjected to neuropathological studies and the changes observed at 2 years are summarized in Table 1. There were numerous spheroids or vacuoles in the axons and neuropil throughout the CNS (Fig. 5) and the peripheral nervous system (PNS) (Fig. 6), indicating the widespread degeneration of axons or synapses. These round or irregular spheroids were 3–90 μm in diameter. The larger spheroids frequently showed vacuolation, fissures, or rarefaction (Figs. 5*B*,*C*, 6*C*). As summarized in Table 1, the spheroids were most prominent in the tegmentum of the medulla (Fig. 5*B*), the lower pons, and the dorsal horns (Fig. 5*C*) of the entire spinal cord. In addition to the spheroids, vacuoles of various sizes (3–40 μm in diameter) were observed (Fig. 5*B*,*C*,*L*). Most of the larger vacuoles had a core (Fig. 5*B*,*C*). A single irregularly swollen axon that contained both spheroids and a vacuole was detected in a longitudinal section (Fig. 6*C*). The cerebral cortex contained numerous vacuoles, most of which were rather small (3–5 μm), and there were only a few spheroids (Fig. 5*L*). Younger $iPLA_2\beta^{-/-}$ mice were also subjected to neuropathological examination and the following data were obtained. At 15 weeks, tiny vacuoles were frequently observed in the molecular layer of the cerebellum (Fig. 5*I*), which became atrophic at 2 years (Fig. 5*H*), and spheroids were also found in the dentate nucleus of the cerebellum (Fig. 5*J*). In other regions, vacuoles and spheroids were only rarely observed. At 32 weeks, some small vacuoles were found in the cerebral cortex, striatum, and hippocampus, and a number of spheroids and large vacuoles were observed in the tegmentum of the lower pons or medulla and in the spinal cord, as well as the cerebellum (data not shown). At 55 weeks, vacuoles or spheroids were distributed throughout the CNS (data not shown). PAS staining revealed many PAS-positive granules, mainly in the normal-looking axons of larger neurons such as anterior horn cells, where very few spheroids or vacuoles were found at 15 weeks (Fig. 5*E*). At 2 years, PAS-positive granules were also scattered in axons or the neuropil where spheroids were prominent (Fig. 5*F*). Both spheroids and vacuoles frequently contained PAS-positive granules (Fig. 5*C*). Although many of the spheroids were positive for PAS to some extent, spheroids were not stained by Berlin blue, which detects iron (data not shown). In $iPLA_2\beta^{+/+}$ mice, a few spheroids and vacuoles were observed exclusively in the gracile nucleus and part of the cuneate nucleus (data not shown), which might have represented physiological neuroaxonal dystrophy occurring as part of the normal aging process.

Immunohistochemistry using an anti-phosphorylated neurofilament antibody (SMI31) revealed strong staining of some small spheroids, indicating that these structures originated from axons (Fig. 7*A*). Most of the large and irregular spheroids that contained narrow clefts or vacuoles were almost completely negative for this antibody, suggesting that severe degeneration had occurred. Some of the spheroids and vacuoles were also stained by anti-ubiquitin antibody, with the cores or fissures of the spheroids and the rims or inner contents of small vacuoles being stained to a varying extent (Fig. 7*B*,*C*). These findings indicate that some of the spheroids and vacuoles contained ubiquitinated proteins.

Morphological analysis of the sciatic nerve demonstrated that the total number of myelinated fibers (density by area) was significantly reduced in $iPLA_2\beta^{-/-}$ mice (Table 2). The density of

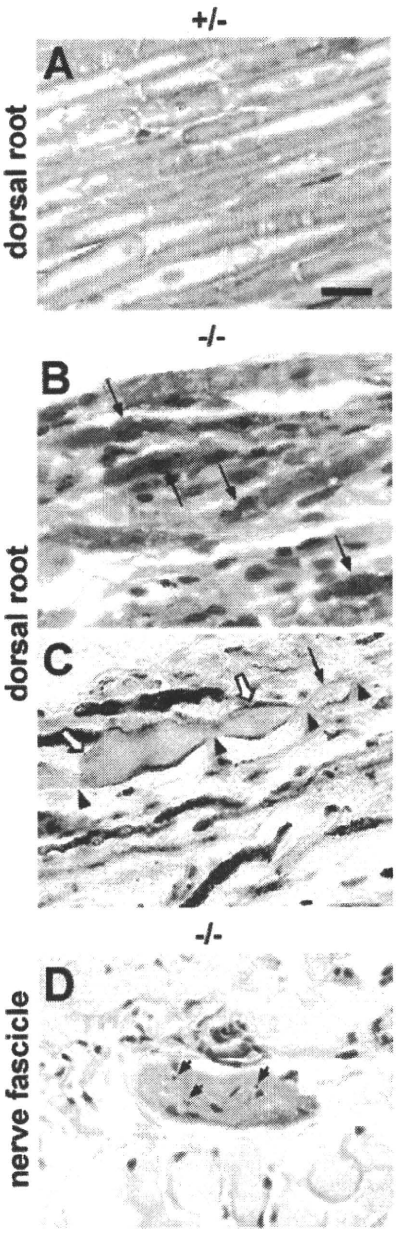

Figure 6. Pathological changes of the PNS. ***A–C***, Dorsal root of an *iPLA$_2\beta^{+/-}$* mouse (***A***) and an *iPLA$_2\beta^{-/-}$* mouse (***B***, ***C***) at 2 years. ***D***, Subcutaneous nerve fascicle of an *iPLA$_2\beta^{-/-}$* mouse at 2 years. ***A***, ***B***, and ***D*** are PAS stained. ***C***, Bielschowsky stain. Scale bar, 16 μm. ***A***, Axons of the *iPLA$_2\beta^{+/-}$* mouse are PAS negative, although the myelin sheath is weakly stained by PAS. ***B***, Swollen axons (arrows) are heterogeneously stained by PAS and contain strongly PAS-positive granules. ***C***, A single swollen axon contains both spheroids (open arrows) and a vacuole (arrow). The central parts of the spheroids (open arrows) are rarefied. Staining of the axonal structures (arrowheads) between the spheroids is weak. ***D***, PAS-positive granules can be seen in the nerve fascicle.

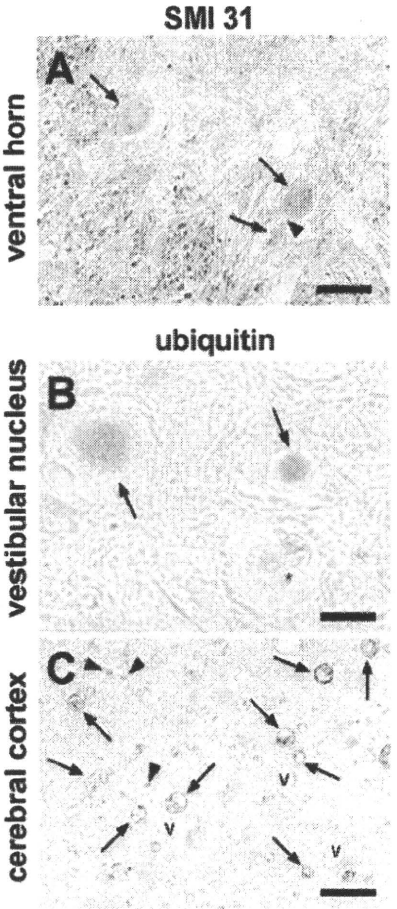

Figure 7. Immunohistochemical analysis of spheroids and vacuoles in *iPLA$_2\beta^{-/-}$* mice at 2 years. ***A***, Ventral horn was stained with anti-phosphorylated neurofilament H (SMI31). ***B***, ***C***, Vestibular nucleus (***B***) and cerebral cortex (***C***) were stained with anti-ubiquitin antibody. v, Vessels. Scale bars: ***A***, 20 μm; ***B***, 10 μm; ***C***, 16 μm. ***A***, Spheroids (arrows) are positive for SMI31, whereas the axonal portion between the spheroids (arrowhead) is negative. ***B***, Two spheroids (arrows) have positive cores. The other spheroid (asterisk) contains vacuoles that are weakly stained or unstained for ubiquitin. ***C***, Numerous vacuoles (arrows) and tiny circles (arrowheads) that are ubiquitin positive in the neuropil of the cerebral cortex.

myelinated fibers was similar (Table 2, supplemental Fig. 2*C*,*D*, available at www.jneurosci.org as supplemental material) in both groups, but the area of the nerve fascicles was significantly smaller in *iPLA$_2\beta^{-/-}$* mice (Table 2, supplemental Fig. 2*B*, available at www.jneurosci.org as supplemental material), indicating that the sciatic nerves of these mice had undergone atrophy because of neuronal degeneration.

Ultrastructural examination of *iPLA$_2\beta^{-/-}$* mice at 55 weeks showed that spheroids in the dorsal funiculus contained tubulovesicular structures, as well as vacuoles, vesicles, and amorphous matrix (Fig. 8). These tubulovesicular structures were also found in the cerebral cortex (data not shown).

Discussion

We showed that iPLA$_2\beta$ deficiency in mice led to motor impairment, which was accompanied by the appearance of axonal swelling (spheroids) and vacuoles throughout the nervous system. Our results provide experimental evidence that iPLA$_2\beta$ plays a critical role in maintaining the structural and functional integrity of axons or synapses, and that iPLA$_2\beta$ dysfunction leads to the occurrence of neuroaxonal dystrophy.

In this study, we found that *iPLA$_2\beta^{-/-}$* mice initially developed normally, but began to show significant motor dysfunction from the age of ~50 weeks (Fig. 4*D*), which progressed to ataxia and weakness by 2 years. These observations indicate that iPLA$_2\beta$ has an important role in maintaining the function of the nervous system, but not in nervous system development. INAD is caused by mutation of the *iPLA$_2\beta$* gene (Khateeb et al., 2006; Morgan et al., 2006) and patients develop the initial symptoms, including hypotonia, areflexia, or weakness < 2 years old. As the disease progresses, dementia, ataxia, blindness, and spasticity occur, and

Table 2. Morphological analysis of sciatic nerves between iPLA$_2\beta^{+/+}$ and iPLA$_2\beta^{-/-}$ mice

	Density of myelinated fibers (per mm^2)	Total area of nerve fascicles (mm^2)	Number of myelinated fibers (density × area)
+/+ ($n = 4$)	20156 ± 4007	0.189 ± 0.037	3735 ± 554
−/− ($n = 7$)	22922 ± 1695	0.136 ± 0.117	3115 ± 234
		($p < 0.05$)	($p < 0.05$)

The number of myelinated fibers per unit area was counted in sciatic nerves. Mice aged 95–103 weeks old were examined. p values were calculated using the Student's t test.

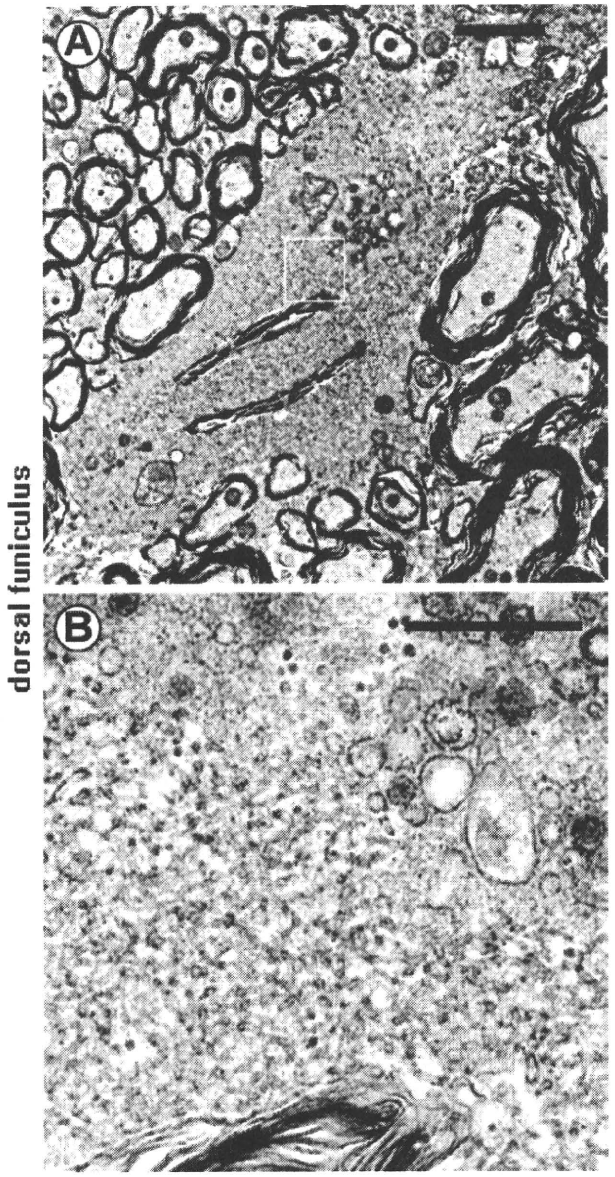

Figure 8. Electron microscopic features of spheroids. ***A***, ***B***, Dorsal funiculus of a *iPLA$_2\beta^{-/-}$* mouse at 56 weeks. ***B*** shows a higher magnification of the boxed region in ***A***. Tubulovesicular structures can be seen in the spheroid, as well as degenerated vesicles and vacuoles. Scale bars: ***A***, 2 μm; ***B***, 0.5 μm.

these patients die before puberty (Nardocci et al., 1999). Although some symptoms, such as weakness and ataxia, were common to INAD patients and *iPLA$_2\beta^{-/-}$* mice, the clinical course was different. In mice, the onset was late and disease progression was slow. The different clinical pictures could possibly be explained by species differences or compensation for iPLA$_2\beta$ deficiency by other PLA$_2$ isotypes (such as iPLA$_2\gamma$) in mice.

However, the neuropathological features seen in *iPLA$_2\beta^{-/-}$* mice were very similar to those found in patients with INAD. Neuroaxonal dystrophy in INAD and NBIA is characterized by a morphological change of axons in the CNS, which is the development of spheroids (Seitelberger, 1952). Numerous spheroids and vacuoles were distributed throughout the CNS in the *iPLA$_2\beta^{-/-}$* mice (Table 1), as is also observed in INAD. As has been reported for INAD (Gonatas et al., 1967), the spheroids were located in the axons and synapses of *iPLA$_2\beta^{-/-}$* mice (Figs. 5, 6). In addition, the cerebellum (which is one of the most susceptible regions in INAD) (Nardocci et al., 1999) seemed to be affected quite early among the CNS regions in *iPLA$_2\beta^{-/-}$* mice (Fig. 5*I*,*J*). Furthermore, examination of the sciatic nerves of *iPLA$_2\beta^{-/-}$* mice showed peripheral nerve degeneration (Table 2, supplemental Fig. 2, available at www.jneurosci.org as supplemental material), as also occurs in INAD (Duncan et al., 1970). Moreover, tubulovesicular structures, which are a characteristic finding in INAD patients (Gonatas et al., 1967), were detected in *iPLA$_2\beta^{-/-}$* mice by electron microscopy (Fig. 8). Because the pathological changes of the nervous system were almost identical, the *iPLA$_2\beta^{-/-}$* mouse seems to be an appropriate model for studying the detailed pathogenesis of neuroaxonal dystrophy in INAD.

The mechanisms leading to the formation of spheroids and vacuoles in the absence of functional iPLA$_2\beta$ remain unclear, but these structures seem to arise from the degeneration of axons or synaptic terminals. Some of the large vacuoles presumably developed from the resorption of spheroids (Cowen and Olmstead, 1963) via a process involving ubiquitination (Fig. 7*B*). Because numerous PAS-positive granules appeared in the axons or neuropil by 15 weeks, which was before the spheroids and vacuoles formed (Fig. 5*E*), and because both spheroids and large vacuoles contained PAS-positive granules (Figs. 5*C*, 6*B*), these granules might be the key to elucidating the pathogenesis of neuroaxonal degeneration in *iPLA$_2\beta^{-/-}$* mice and INAD patients. Because PAS stains materials containing aldehydes as well as staining polysaccharides like glycogen, the PAS-positive material might represent accumulations of polysaccharides, aberrantly glycated proteins, or aldehyde products of lipid peroxides created by an increase of ROS in the iPLA$_2\beta$-deficient state.

iPLA$_2\beta$ is an important enzyme for maintaining phospholipid membranes through the processes of phospholipid turnover, remodeling, and repair (Ma and Turk, 2001). Therefore, iPLA$_2\beta$ deficiency may alter the phospholipid composition of cellular and subcellular membranes, or may lead to failure to repair oxidative damage to membrane phospholipids, resulting in changes of membrane permeability, fluidity, or ion homeostasis. Why are the axons or presynaptic terminals, and not the cytoplasm, selectively affected in INAD patients and *iPLA$_2\beta^{-/-}$* mice? The tubulovesicular structures observed in both INAD patients and *iPLA$_2\beta^{-/-}$* mice (Fig. 8) are believed to result from degenerated ER or mitochondria. iPLA$_2\beta$ has been reported to exist in and protect mitochondria (Seleznev et al., 2006), as well as being abundant in neurites and axon terminals (Ong et al., 2005), so its absence would contribute to damage targeting mitochondria in

axons and synaptic terminals, leading to degeneration of the axons and synaptic terminals.

Some individuals with NBIA, formerly known as Hallervorden-Spatz syndrome, have a mutation of the pantothenate kinase 2 (*PANK2*) gene (Zhou et al., 2001). The product of this gene is an enzyme localized to the mitochondria (Kotzbauer et al., 2005) and involved in the biosynthesis of coenzyme A (CoA), which has various roles that include acting as a carrier of free fatty acids. Oxidative damage or impaired fatty acid metabolism resulting from mitochondrial CoA deficiency is thought to be a possible cause of neurodegenerative changes (Johnson et al., 2004). The common mechanism of neuroaxonal dystrophy in iPLA$_2\beta$ deficiency and PANK2 deficiency may be mitochondrial dysfunction affecting the axons and/or axon terminals. Clarification of the pathogenesis of neuroaxonal dystrophy in *iPLA$_2\beta^{-/-}$* mice will hopefully lead to the development of treatments for INAD and other neurodegenerative disorders.

References

Balboa MA, Varela-Nieto I, Killermann Lucas K, Dennis EA (2002) Expression and function of phospholipase A(2) in brain. FEBS Lett 531:12–17.

Bao S, Miller DJ, Ma Z, Wohltmann M, Eng G, Ramanadham S, Moley K, Turk J (2004) Male mice that do not express group VIA phospholipase A2 produce spermatozoa with impaired motility and have greatly reduced fertility. J Biol Chem 279:38194–38200.

Cowen D, Olmstead EV (1963) Infantile neuroaxonal dystrophy. J Neuropathol Exp Neurol 22:175–236.

Duncan C, Strub R, McGarry P, Duncan D (1970) Peripheral nerve biopsy as an aid to diagnosis in infantile neuroaxonal dystrophy. Neurology 20:1024–1032.

Farooqui AA, Ong WY, Horrocks LA (2004) Biochemical aspects of neurodegeneration in human brain: involvement of neural membrane phospholipids and phospholipases A2. Neurochem Res 29:1961–1977.

Gonatas NK, Evangelista I, Walsh GO (1967) Axonic and synaptic changes in a case of psychomotor retardation: an electron microscopic study. J Neuropathol Exp Neurol 26:179–199.

Inoue N, Ikawa M, Isotani A, Okabe M (2005) The immunoglobulin superfamily protein Izumo is required for sperm to fuse with eggs. Nature 434:234–238.

Johnson MA, Kuo YM, Westaway SK, Parker SM, Ching KH, Gitschier J, Hayflick SJ (2004) Mitochondrial localization of human PANK2 and hypotheses of secondary iron accumulation in pantothenate kinase-associated neurodegeneration. Ann NY Acad Sci 1012:282–298.

Khateeb S, Flusser H, Ofir R, Shelef I, Narkis G, Vardi G, Shorer Z, Levy R, Galil A, Elbedour K, Birk OS (2006) PLA2G6 mutation underlies infantile neuroaxonal dystrophy. Am J Hum Genet 79:942–948.

Kotzbauer PT, Truax AC, Trojanowski JQ, Lee VM (2005) Altered neuronal mitochondrial coenzyme A synthesis in neurodegeneration with brain iron accumulation caused by abnormal processing, stability, and catalytic activity of mutant pantothenate kinase 2. J Neurosci 25:689–698.

Ma Z, Turk J (2001) The molecular biology of the group VIA Ca^{2+}-independent phospholipase A2. Prog Nucleic Acid Res Mol Biol 67:1–33.

Mancuso DJ, Jenkins CM, Gross RW (2000) The genomic organization, complete mRNA sequence, cloning, and expression of a novel human intracellular membrane-associated calcium-independent phospholipase A(2). J Biol Chem 275:9937–9945.

Matsuoka Y, Matsuoka Y, Shibata S, Ban T, Toratani N, Shigekawa M, Ishida H, Yoneda Y (2002) A chromodomain-containing nuclear protein, MRG15 is expressed as a novel type of dendritic mRNA in neurons. Neurosci Res 42:299–308.

Morgan NV, Westaway SK, Morton JE, Gregory A, Gissen P, Sonek S, Cangul H, Coryell J, Canham N, Nardocci N, Zorzi G, Pasha S, Rodriguez D, Desguerre I, Mubaidin A, Bertini E, Trembath RC, Simonati A, Schanen C, Johnson CA, et al. (2006) PLA2G6, encoding a phospholipase A(2), is mutated in neurodegenerative disorders with high brain iron. Nat Genet 38:752–754.

Nardocci N, Zorzi G, Farina L, Binelli S, Scaioli W, Ciano C, Verga L, Angelini L, Savoiardo M, Bugiani O (1999) Infantile neuroaxonal dystrophy: clinical spectrum and diagnostic criteria. Neurology 52:1472–1478.

Ong WY, Yeo JF, Ling SF, Farooqui AA (2005) Distribution of calcium-independent phospholipase A2 (iPLA 2) in monkey brain. J Neurocytol 34:447–458.

Seitelberger F (1952) Eine unbekannte Form von infantiler Lipoidspeicher-Krankheit des Gehirns. Proc 1st Int Congr Neuropathol 3:323–333.

Seleznev K, Zhao C, Zhang XH, Song K, Ma ZA (2006) Calcium-independent phospholipase A2 localizes in and protects mitochondria during apoptotic induction by staurosporine. J Biol Chem 281:22275–22288.

Shinzawa K, Tsujimoto Y (2003) PLA2 activity is required for nuclear shrinkage in caspase-independent cell death. J Cell Biol 163:1219–1230.

Six DA, Dennis EA (2000) The expanding superfamily of phospholipase A(2) enzymes: classification and characterization. Biochim Biophys Acta 1488:1–19.

Sumi H, Nagano S, Fujimura H, Kato S, Sakoda S (2006) Inverse correlation between the formation of mitochondria-derived vacuoles and Lewy-body-like hyaline inclusions in G93A superoxide-dismutase-transgenic mice. Acta Neuropathol (Berl) 112:52–63.

Tang J, Kriz RW, Wolfman N, Shaffer M, Seehra J, Jones SS (1997) A novel cytosolic calcium-independent phospholipase A2 contains eight ankyrin motifs. J Biol Chem 272:8567–8575.

Yang HC, Mosior M, Ni B, Dennis EA (1999) Regional distribution, ontogeny, purification, and characterization of the Ca^{2+}-independent phospholipase A2 from rat brain. J Neurochem 73:1278–1287.

Zhong Y, Takemoto M, Fukuda T, Hattori Y, Murakami F, Nakajima D, Nakayama M, Yamamoto N (2004) Identification of the genes that are expressed in the upper layers of the neocortex. Cereb Cortex 14:1144–1152.

Zhou B, Westaway SK, Levinson B, Johnson MA, Gitschier J, Hayflick SJ (2001) A novel pantothenate kinase gene (PANK2) is defective in Hallervorden-Spatz syndrome. Nat Genet 28:345–349.

J Neuropathol Exp Neurol

Vol. 68, No. 1
January 2009
pp. 37–47

ORIGINAL ARTICLE

Nuclear TAR DNA Binding Protein 43 Expression in Spinal Cord Neurons Correlates With the Clinical Course in Amyotrophic Lateral Sclerosis

Hisae Sumi, MD, PhD, Shinsuke Kato, MD, PhD, Yuko Mochimaru, Harutoshi Fujimura, MD, PhD, Masaki Etoh, MD, PhD, and Saburo Sakoda, MD, PhD

Abstract

TAR DNA binding protein 43 (TDP-43) has been considered a signature protein in frontotemporal dementia and amyotrophic lateral sclerosis (ALS), but not in ALS associated with the superoxide dismutase 1 (*SOD1*) gene mutations (ALS1). To clarify how TDP may be involved in ALS pathogenesis, clinical and pathological features in cases of sporadic ALS ([SALS] n = 18) and ALS1 (n = 6) were analyzed. In SALS patients with rapid clinical courses, TDP mislocalization (i.e. cytoplasmic staining and TDP-positive cytoplasmic inclusions) in anterior horn cells was frequent. In SALS patients with slow clinical courses, TDP-43 mislocalization was rare. In an ALS1 patient with the *SOD1* gene mutation C111Y, there were numerous TDP-positive inclusions and colocalization of SOD1 and TDP. In mutant SOD1 transgenic (G93A) mice at the end stage (median, 256 days), TDP-positive inclusions and TDP colocalization with SOD1 were also observed; nuclear TDP-43 immunoreactivity was highly correlated with life span in these mice. In both humans and mice, nuclei that stained strongly for TDP were large and circular; weakly stained nuclei were atrophic or deformed. In conclusion, low levels of TDP expression in the nucleus cor relate with a rapid clinical course in SALS and in ALS1 model mice, suggesting that nuclear TDP may play a protective role against motor neuron death resulting from different underlying etiologies.

Key Words: Amyotrophic lateral sclerosis, ALS, Anterior horn cell, ALS1, G93A transgenic mice, Lewy body–like hyaline inclusion, SOD1, TDP-43.

INTRODUCTION

Amyotrophic lateral sclerosis (ALS) is a fatal motor neuron disease that causes progressive motor paralysis. The underlying pathogenetic mechanisms are largely unknown in 90% of ALS patients, that is, those with sporadic ALS (SALS). Of the 10% of ALS cases with familial ALS (FALS), approximately one fifth are associated with a mutation in the superoxide dismutase 1 (*SOD1*) gene; these patients are classified as ALS1 (1, 2). The pathogenesis of ALS1 is thought to involve aggregation of mutant SOD1 and subsequent oxidative stress (3). Another rare cause of juvenile autosomal recessive FALS is the gene that encodes ALS2, also known as alsin (4, 5). In most cases of FALS, however, the causative gene has not been identified because of low penetrance.

TAR DNA binding protein 43 (TDP-43), a nuclear protein, contains 2 fully functional RNA recognition motif domains and a C-terminal region that is capable of binding directly to several proteins of the heterogeneous nuclear ribonucleoprotein family (6–8); these ribonucleoproteins have a variety of functions including the modification, stabilization, and transport of RNA. The TDP modifies the splicing of exon 9 of the cystic fibrosis transmembrane conductance regulator gene (9) and of exon 3 of the apolipoprotein A-II gene (10). Recently, it also has been reported that loss of TDP in vitro results in nuclear dysmorphism, misregulation of the cell cycle, and apoptosis (11).

Neuronal inclusions, such as Lewy body–like hyaline inclusions (LBHIs), or the aggregation of mutant SOD1 in ALS1 (3, 12) are known to be important pathological features in the pathogenesis of neurodegenerative diseases. The TDP is a component of the ubiquitin-positive inclusions and neurites observed in frontotemporal dementia and ALS (13, 14). The TDP-positive round or filamentous inclusions in the cytoplasm and mislocalization of TDP from the nucleus to the cytoplasm have been observed in all cases of SALS (15) and FALS, but not in ALS1 (16, 17). A novel missense mutation in TDP was recently identified as causative in familial motor neuron disease and SALS (18, 19). Although the concept of TDP proteinopathy has been suggested (14, 20), the presence of TDP-positive inclusions in other diseases, including hippocampal sclerosis, Alzheimer disease (21), Parkinson disease (22), Pick disease (23), and neoplastic lesions (24), complicates this issue. Furthermore, Sanelli et al (25) have reported that TDP is not a major ubiquitinated target within the pathological inclusions of ALS.

From the Department of Neurology, Osaka University Graduate School of Medicine (HS, ME, SS), Yamadaoka, Suita; Department of Neuropathology, Institute of Neurological Sciences, Faculty of Medicine, Tottori University (SK), Nishi-cho, Yonago; Department of Health Science, Osaka University Graduate School of Medicine (YM), Yamadaoka, Suita; and Department of Neurology, Toneyama National Hospital (HF), Toneyama, Toyonaka, Japan.

Send correspondence and reprint requests to: Hisae Sumi, MD, PhD, Department of Neurology, Osaka University Graduate School of Medicine, 2-2 Yamadaoka, Suita, 565-0871, Japan; E-mail: hasumi@neurol.med.osaka-u.ac.jp

This study was supported by the Health and Labor Sciences Research on Measures for Incurable Disease, Ministry on Health, Labor and Welfare of Japan.

TABLE. Clinical and Pathological Data*

Patients	Age, years	Disease Duration, years	Initial Weakness Manifestation	Use of Respirator (Estimated Duration)	Cause of Death	Family History	No. Large Neurons†	No. Large Neurons With TDP Mislocalization†	No. Neuronal Inclusions†	No. Glial Inclusions†
SALS r-1	69	0.7	L	No	Pneumonia	No	13	6 (I)	40	16
SALS r-2	77	0.8	U	No	Resp. f.	No	23	8 (I>D)	34	4
SALS r-3	49	0.8	L, B	No	Resp. f.	No	9	4 (I)	35	6
SALS r-4	60	1.5	B, U	No	Pneumonia	No	36	12 (D>I)	25	38
SALS r-5	59	1.5	U	No	Resp. f.	No	16	9 (D>I)	12	22
SALS r-6	69	2	B, U	No	Resp. f.	No	22	12 (D>I)	25	38
SALS r-7	51	2	B	No	Resp. f.	No	22	11 (D>I)	21	11
SALS r-8	71	2	U	No	Resp. f.	No	21	4 (I>D)	69	8
SALS r-9	61	2	U	No	Resp. f.	No	8	3 (I>D)	12	9
SALS r-10	64	2	L	No	Pneumonia	No	7	0	9	123
SALS r-11	73	2.5	B	No	Resp. f.	No	25	4 (I>D)	14	7
SALS r-12	60	2.5	B, U	No	Resp. f.	No	12	7 (D>I)	18	19
SALS r-13	71	2.5	U	No	Resp. f.	No	4	0	26	26
SALS s-1	79	5	U	No	Resp. f.	No	2	0	0	0
SALS s-2	53	5.5	U	No	Resp. f.	No	9	0	4	2
SALS s-3	63	5.5	U, L	No	Resp. f.	No	4	0	2	2
SALS s-4	48	6.7	?	No	Resp. f.	No	15	0	0	2
SALS s-5	45	7.3	?	No	Resp. f.	No	2	0	0	3
				Median (range), 62 (45–79); 2.0 (0.7–7.3)						
ALS1-1 (C111Y)	71	7	L	3 years	Ren f.	Yes	0	0	20	31
ALS1-2 (126 2bp del)	42	2	L	0.5 years	Pneumonia	Yes	3	1 (D)	0	0
ALS1-3 (126 2bp del)	65	11	L	10 years	Hemorrhage	Yes	0	0	0	0
ALS1-4 (G37R)	50	9	U	2.5 years	Pneumonia	Yes	1	0	0	0
ALS1-5 (L126S)	67	9	L	No	Resp. f.	Yes	13	0	0	0
ALS1-6 (L126S)	45	8.5	L	No	Resp. f.	Yes	7	0	0	0
				Median (range), 58 (42–71); 9 (2–11)						

*ALS1, amyotrophic lateral sclerosis (*SOD-1* gene mutation); B, bulbar; D, diffuse staining pattern; D > I, predominantly diffuse staining pattern; I, inclusion pattern; I > D, predominantly inclusion pattern; L, lower limb; Ren. f., renal failure; Resp. f., respiratory failure; SALS r, sporadic ALS with a rapid clinical course (i.e. ≤2.5 years); SALS s, SALS with a slow clinical course; U, upper limb.

†Large neurons with cytoplasm exceeding 37 μm in diameter and clear nucleoli were counted. TAR DNA binding protein (TDP) mislocalization includes a diffuse staining pattern in the cytoplasm (D) and TDP-positive inclusions in the cytoplasm (I). Cell types containing TDP-positive inclusions were estimated as neuronal or glial on the basis of the morphology of their nuclei and cytoplasm.

To clarify how TDP may be involved in pathogenetic mechanisms in ALS, we examined SALS and ALS1 patients clinically and pathologically by immunohistochemistry using an anti-TDP antibody. We also examined the lumbar spinal cords of mutant SOD1 transgenic mice (G93A mice) that have lower copy numbers of the mutant *SOD1* gene than the G93A mice previously examined by Robertson et al (26); G93A mice with low copy numbers of the mutant *SOD1* gene show pathological changes that are similar to those in patients with ALS (27).

MATERIALS AND METHODS

ALS Cases and Pathological Assessment

Fixed paraffin-embedded 4-μm-thick sections through the lumbar spinal cord at the L5 level were obtained from Osaka University Graduate School of Medicine (Suita) for clinicopathologic analysis. These patients had SALS (n = 18; age at death 62 [median, 45–79] years; disease duration, 2 [0.7–7.3] years) or ALS1 (n = 6; age at death, 58 [42–71] years; disease duration, 9 [2–11] years; Table). All neuropathologic analyses were performed by trained neuropathologists. Sporadic ALS patients who did and did not have a history of respirator use and whose deaths were caused by respiratory failure or pneumonia were examined. Clinical data including the localization of initial symptoms, history of respirator use, cause of death, and family history are shown in the Table.

Deparaffinized sections were incubated for 30 minutes with 0.3% hydrogen peroxide to quench endogenous peroxidase activity and then washed with PBS. The primary antibodies used were rabbit polyclonal antibodies against TDP-43 (1:3000, Protein Tech Group, Chicago, IL) and ubiquitin (1:2000, Dako, Glostrup, Denmark), mouse monoclonal antibodies against human SOD1 (0.5 μg/mL, clone 1G2, MBL, Aichi, Japan) and phosphorylated neurofilament (1:10,000, SMI31, Covance, Berkeley, CA), and a sheep polyclonal antibody against human SOD1 (1:20,000, Calbiochem, San Diego, CA); these were applied to serial sections as primary antibodies. Goat anti-rabbit and anti-mouse immunoglobulins conjugated to peroxidase-labeled dextran polymer (ready to use, Dako Envision+, Dako Corp, Carpinteria, CA) and rabbit anti-sheep immunoglobulin (1:1000, Abcam PLC, Cambridge, United Kingdom) were used as secondary antibodies. Reaction products were visualized with 3,3′-diaminobenzidine tetrahydrochloride (ImmPACT DAB, Vector Laboratories, Burlingame, CA), and hematoxylin was used to counterstain cell nuclei.

To estimate the numbers of TDP-positive cytoplasmic inclusions, large neurons that had clear nucleoli and cell bodies with a diameter greater than 37 μm (28) (presumed to be α motoneurons) and the numbers of neurons with TDP mislocalization from the nucleus to the cytoplasm in the gray matter, from video images of each section obtained with a digital camera (Keyence VB-7010, Keyence, Osaka) attached to a light microscope (EclipseE800, Nikon, Tokyo), were counted. The diameters of the neurons were measured with the aid of image analysis software (VH-H1A5, Keyence). Mislocalization of TDP was defined as the presence of a TDP-negative nucleus and TDP-positive cytoplasm. In mislocalizations of TDP, there can also be diffuse staining patterns in the cytoplasm and TDP-positive filamentous or round inclusions in the cytoplasm. Cells containing TDP-positive inclusions were classified as neurons or glia on the basis of the shape of their nuclei and cytoplasm.

Animals

Transgenic mice expressing the mutated human *SOD1* (G93A) gene at a low level (B6SJL-TgN[SOD1]-G93A)1Gur^{dl} [G1L]) were obtained from Jackson Laboratory (Bar Harbor, ME). These mice carry 18 transgene copies because of a reduction in the copy number compared with (B6SJL-TgN[SOD1]-G93A)1Gur (G1H) mice, which express 25 copies (3). The G1L mice were bred and maintained as hemizygotes by mating with wild-type B6.SJL mice. Non-transgenic littermates were used as controls. All animals were genotyped and handled as previously described (29). We examined control (n = 6,292 [median, 240–296] days old) and G1L (n = 9,256 [224–281] days old, end stage) mice. One G1H mouse (120 days, end stage), also obtained from Jackson Laboratory, was examined to confirm the lack of TDP-43 abnormalities reported previously (26). *End stage* was defined as occurring when the mouse was so severely paralyzed that it could hardly move or drink water. The mice were killed with an overdose of sodium pentobarbital and perfused with PBS followed by 4% paraformaldehyde. The lumbar enlargement of the spinal cord was removed, immersed in 4% paraformaldehyde overnight at 4°C, and then dehydrated and embedded in paraffin blocks. Paraffin sections, 4-μm-thick, were prepared and stained with hematoxylin and eosin. Every fifth section (cut at 20-μm intervals) was obtained, and 4 sections from each mouse were used to count the total number of LBHIs in the sections. For immunohistochemistry, the primary antibodies used on the serial sections were against TDP-43 (1:600, Protein Tech Group) and human SOD1 (0.5 μg/mL, clone 1G2, MBL, Nagoya, Japan).

Semiquantitative Analysis of Immunoreactivity for TDP

Because variation in the TDP immunoreactivity (TDP-IR) was evident among G1L mice, the patterns of TDP immunostaining were divided into normal (0) and abnormal (1 to 4), the latter showing TDP-positive neurites and inclusions and varying degrees of nuclear positivity. The stages of normal or abnormal patterns were classified by TDP-IR of the neuron nuclei as follows: normal pattern (Stage 0): same as in normal littermates, with immunoreactivity apparent only in nuclei; abnormal pattern (Stages 1–4): Stage 1, weak immunoreactivity in nuclei; Stage 2, weak to moderate immunoreactivity in nuclei; Stage 3, moderate to strong immunoreactivity in nuclei; Stage 4, strong immunoreactivity in nuclei.

Quantitative Analysis of LBHIs

The numbers of LBHIs with a core and halo in neurons of the lumbar spinal cord were counted in hematoxylin and

eosin–stained sections (100× objective) from each G1L mouse as previously described (29).

Statistical Analysis

Differences in the numbers of TDP-positive inclusions in neurons and glia and in large neurons (>37 μm) between SALS patients with a rapid course and those with a slow course were analyzed by Wilcoxon rank sum test. The relationships among the numbers of large neurons and TDP-positive inclusions in neurons and glia were also analyzed using Spearman correlation coefficient with a 95% confidence interval (CI). In G1L mice, the relationships among age at the end stage, number of LBHIs, and TDP-IR were analyzed using Spearman correlation coefficient with 95% CI. Exploratory subgroup analyses for age at the end stage were done in the TDP-IR weak groups (Stages 1 and 2) and the TDP-IR strong groups (Stages 3 and 4) by Kolmogorov-Smirnov test. All statistical analyses were performed with SAS version 9.1 (SAS Institute Inc, Cary, NC).

RESULTS

ALS Cases

In the lumbar cords of SALS patients with disease durations less than or equal to 2.5 years (SALS r-1 to -13), mislocalization of TDP was frequently observed (Figs. 1B, C; Table); this was not evident in controls (Fig. 1A). There was a diffuse cytoplasmic staining pattern, especially in large neurons (>37 μm, Fig. 1B) and TDP-positive filamentous or round inclusions were evident in atrophic neurons and in glia (Figs. 1C, D); the nuclei in the neurons and glia were negative for TDP. In SALS patients with mild to moderate neuronal loss, there was often a diffuse TDP staining pattern in the cytoplasm of large neurons (Table). No extracellular TDP-positive inclusions were apparent. By contrast, in SALS patients with disease durations longer than 5 years (SALS s-1 to -5), neurons with diffuse cytoplasmic staining patterns were not evident, and TDP-positive inclusions were only rarely detected (Table). The TDP-IR of the nuclei of residual neurons appeared to be preserved.

In ALS1 patients, diffuse cytoplasmic TDP staining of large neurons was found only in 1 patient, i.e. ALS1-2 (126 2bp del), who had a clinical course of 2 years (Table). Some small neurons in Patients ALS1-2 and ALS1-3 (126 2bp del) also showed diffuse cytoplasmic TDP staining (Figs. 3A, C). The TDP-positive inclusions were prominent in the glia and in small neurons or their neurites in Patient ALS1-1 (C111Y), who had no remaining large neurons. The nuclei of cells with TDP-positive inclusions were TDP negative (Figs. 2A, E). Colocalization of TDP and SOD1 was frequently evident as

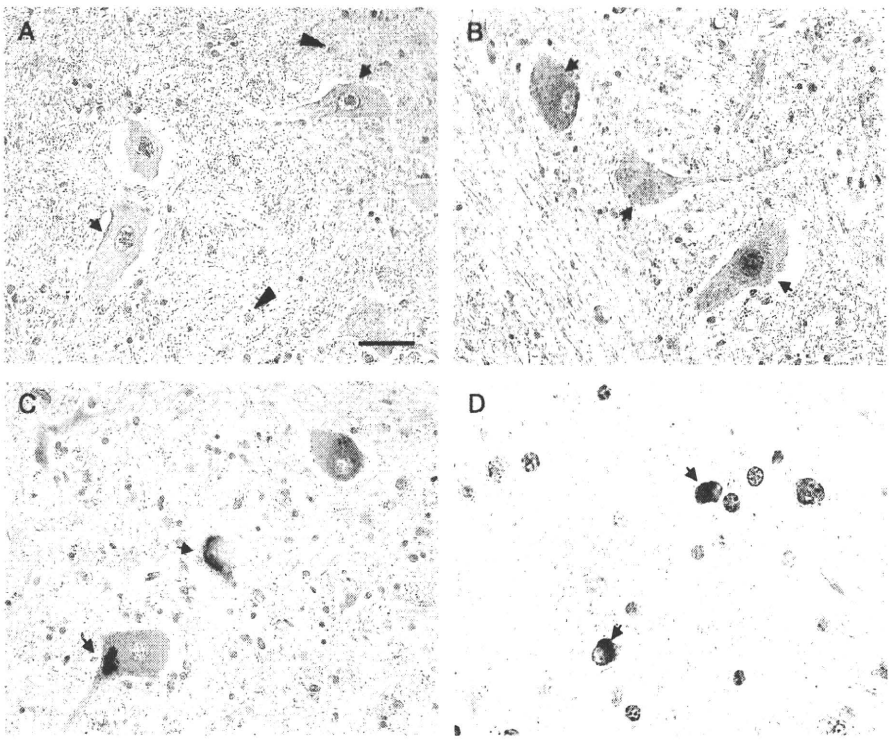

FIGURE 1. Mislocalization of TAR DNA binding protein (TDP) in cases of sporadic amyotrophic lateral sclerosis (SALS) with rapid clinical courses. **(A)** Normal control. The nuclei of large neurons are positive for TDP (arrows). Some glia (arrowheads) are weakly stained. **(B–D)** SALS patients. **(B)** There is diffuse punctate cytoplasmic staining in the neuron on the left (arrow), and heterogeneous staining in the middle (arrow) is observed in the cytoplasm. Nuclei of neurons on the left and in the middle are negative for TDP, whereas the nucleus of the neuron on the right is stained. **(C)** Variable appearances of cytoplasmic TDP inclusions (arrows). The structure on the left (arrow) is rounded, whereas the one in the middle neuron is elongated and filamentous (arrow). **(D)** Glial inclusions are positive for TDP (arrows). Immunohistochemistry against TDP. Scale bar = 50 μm.

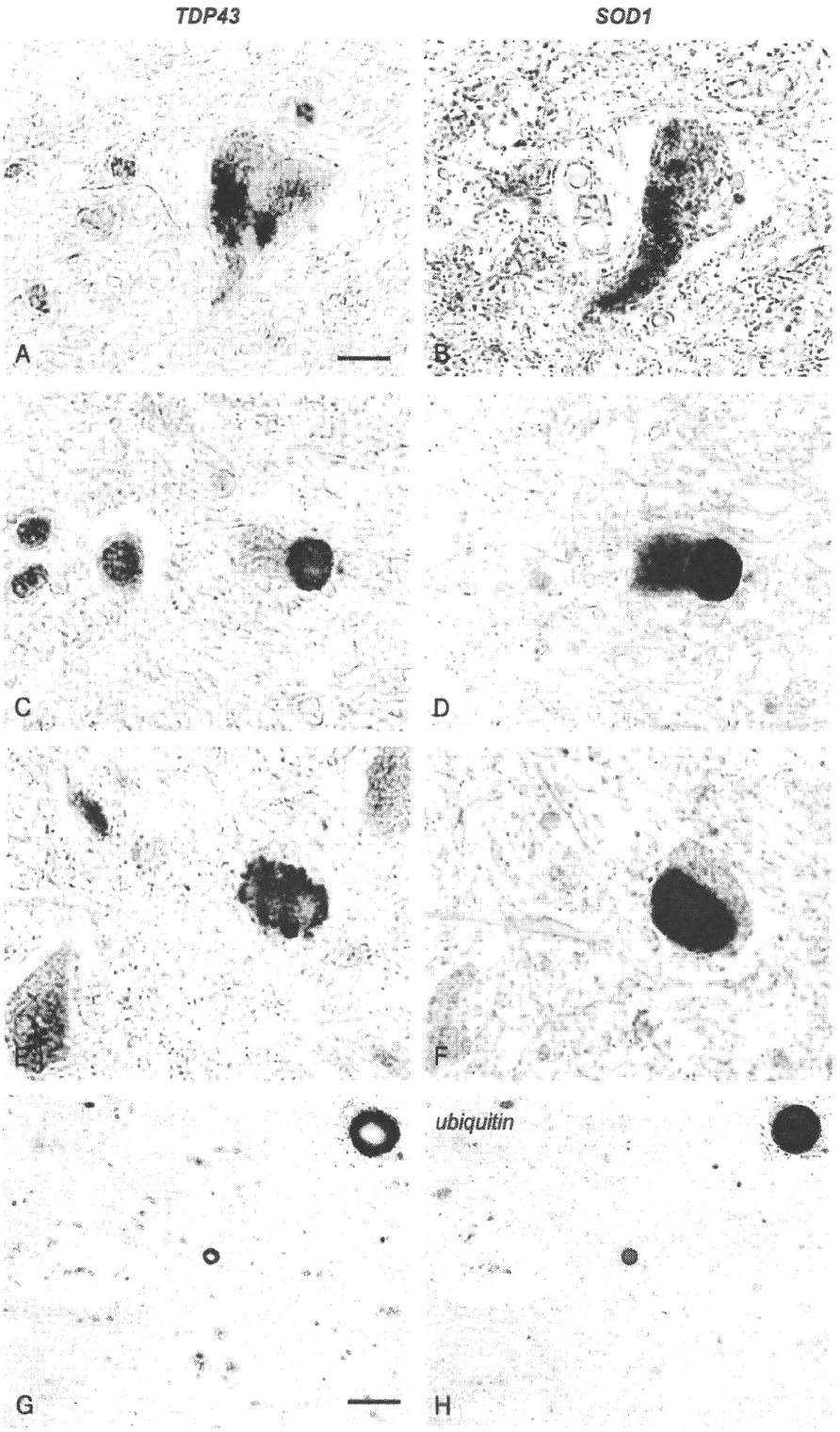

FIGURE 2. Colocalization of TAR DNA binding protein (TDP) and superoxide dismutase 1 (SOD1) in neurons of an amyotrophic lateral sclerosis 1 (C111Y) patient. **(A, B)** Heterogeneous cytoplasmic staining patterns for TDP **(A)** and for SOD1 **(B)**. The nucleus is TDP negative. **(C–F)** Neuronal inclusions are positive for TDP **(C, E)** and SOD1 **(D, F)**. **(G, H)** The halo portion of a Lewy body–like hyaline inclusion (LBHI) is stained strongly for TDP **(G)** and ubiquitin **(H)**. The upper panels are high-magnification views of each LBHI. Immunohistochemistry: **(A, C, E, G)** = TDP; **(B, D, F)** = SOD1; **(H)** = ubiquitin. **(B, D, F,** and **H)** are adjacent serial sections of **(A, C, E,** and **G)**, respectively. Scale bars = **(A–F)** 10 μm; **(G, H)** 50 μm; insets in **(G, H)** = 16 μm.